

Article

## Discovery of a potent, orally bioavailable PI4KIII $\beta$ inhibitor (UCB9608) able to significantly prolong allogeneic organ engraftment in vivo

James Reuberson, Helen Horsley, Richard J Franklin, Daniel Ford, Judi Neuss, Daniel Brookings, Qiuya Huang, Bart Vanderhoydonck, Ling-Jie Gao, Miyeon Jang, Piet Herdewijn, Anant Ghawalkar, Farnaz Fallah-Arani, Adnan Khan, Jamie Henshall, Mark Jairaj, Sarah Malcolm, Eleanor Ward, Lindsay Shuttleworth, Yuan Lin, Shenggiao Li, Thierry Louat, Mark Waer, Jean Herman, Andrew Payne, Tom Ceska, Carl Doyle, William Ross Pitt, Mark Calmiano, Martin Augustin, Stefan Steinbacher, Alfred Lammens, and Rodger Allen

*J. Med. Chem.*, **Just Accepted Manuscript** • DOI: 10.1021/acs.jmedchem.8b00521 • Publication Date (Web): 28 Jun 2018

Downloaded from <http://pubs.acs.org> on June 29, 2018

### Just Accepted

“Just Accepted” manuscripts have been peer-reviewed and accepted for publication. They are posted online prior to technical editing, formatting for publication and author proofing. The American Chemical Society provides “Just Accepted” as a service to the research community to expedite the dissemination of scientific material as soon as possible after acceptance. “Just Accepted” manuscripts appear in full in PDF format accompanied by an HTML abstract. “Just Accepted” manuscripts have been fully peer reviewed, but should not be considered the official version of record. They are citable by the Digital Object Identifier (DOI®). “Just Accepted” is an optional service offered to authors. Therefore, the “Just Accepted” Web site may not include all articles that will be published in the journal. After a manuscript is technically edited and formatted, it will be removed from the “Just Accepted” Web site and published as an ASAP article. Note that technical editing may introduce minor changes to the manuscript text and/or graphics which could affect content, and all legal disclaimers and ethical guidelines that apply to the journal pertain. ACS cannot be held responsible for errors or consequences arising from the use of information contained in these “Just Accepted” manuscripts.

SCHOLARONE™  
Manuscripts

1  
2  
3  
4  
5  
6  
7  
8  
9  
10  
11  
12  
13  
14  
15  
16  
17  
18  
19  
20  
21  
22  
23  
24  
25  
26  
27  
28  
29  
30  
31  
32  
33  
34  
35  
36  
37  
38  
39  
40  
41  
42  
43  
44  
45  
46  
47  
48  
49  
50  
51  
52  
53  
54  
55  
56  
57  
58  
59  
60

1  
2  
3  
4  
5  
6  
7  
8  
9  
10  
11  
12  
13  
14  
15  
16  
17  
18  
19  
20  
21  
22  
23  
24  
25  
26  
27  
28  
29  
30  
31  
32  
33  
34  
35  
36  
37  
38  
39  
40  
41  
42  
43  
44  
45  
46  
47  
48  
49  
50  
51  
52  
53  
54  
55  
56  
57  
58  
59  
60

# Discovery of a potent, orally bioavailable PI4KIII $\beta$ inhibitor (UCB9608) able to significantly prolong allogeneic organ engraftment *in vivo*

*James Reuberson*<sup>\*†</sup>, *Helen Horsley*<sup>†</sup>, *Richard J. Franklin*<sup>†</sup>, *Daniel Ford*<sup>†</sup>, *Judi Neuss*<sup>†</sup>, *Daniel Brookings*<sup>†</sup>, *Qiuya Huang*<sup>‡</sup>, *Bart Vanderhoydonck*<sup>‡</sup>, *Ling-Jie Gao*<sup>‡</sup>, *Mi-Yeon Jang*<sup>‡</sup>, *Piet Herdewijn*<sup>‡</sup>, *Anant Ghawalkar*<sup>¶</sup>, *Farnaz Fallah-Arani*<sup>†</sup>, *Adnan Khan*<sup>†</sup>, *Jamie Henshall*<sup>†</sup>, *Mark Jairaj*<sup>†</sup>, *Sarah Malcolm*<sup>†</sup>, *Eleanor Ward*<sup>†</sup>, *Lindsay Shuttleworth*<sup>†</sup>, *Yuan Lin*<sup>‡</sup>, *Shenggiao Li*<sup>‡</sup>, *Thierry Louat*<sup>‡</sup>, *Mark Waer*<sup>‡</sup>, *Jean Herman*<sup>‡</sup>, *Andrew Payne*<sup>†</sup>, *Tom Ceska*<sup>†</sup>, *Carl Doyle*<sup>†</sup>, *Will Pitt*<sup>†</sup>, *Mark Calmiano*<sup>†</sup>, *Martin Augustin*<sup>♠</sup>, *Stefan Steinbacher*<sup>♠</sup>, *Alfred Lammens*<sup>♠</sup> and *Rodger Allen*<sup>†</sup>.

<sup>†</sup>UCB Pharma, 208 Bath Road, Slough, Berkshire, SL1 3WE, United Kingdom.

<sup>‡</sup>KU Leuven, Interface Valorization Platform, IVAP, Campus ST.-Rafaël, Blok I, 8°, Kapucijnenvoer 33 B 7001, 3000 Leuven, Belgium.

<sup>¶</sup>SAI Life Sciences Ltd, International Biotech Park, Hinjewadi, Pune 411 057, India.

<sup>♠</sup>Proteros Biostructures GmbH, Bunsenstrasse. 7a, 82152 Martinsried, Germany.

1  
2  
3 KEYWORDS Immunosuppressive, allogeneic organ engraftment, Phosphoinositol 4-kinase III $\beta$ ,  
4  
5 transplantation, human mixed lymphocyte reaction, selectivity profile, binding mode, solubility.  
6  
7

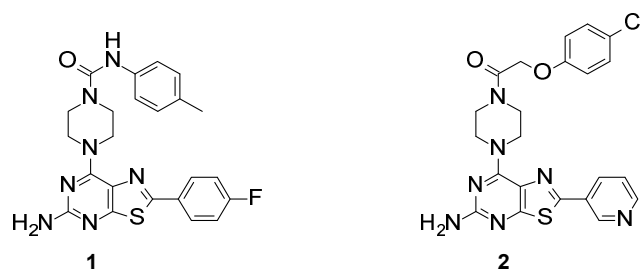
8  
9 ABSTRACT The primary target of a novel series of immunosuppressive 7-piperazin-1-  
10  
11 ylthiazolo[5,4-*d*]pyrimidin-5-amines was identified as the lipid kinase, PI4KIII $\beta$ . Evaluation of  
12  
13 the series highlighted their poor solubility and unwanted off-target activities. A medicinal  
14  
15 chemistry strategy was put in place to optimize physico-chemical properties within the series,  
16  
17 whilst maintaining potency and improving selectivity over other lipid kinases. Compound **22** was  
18  
19 initially identified and profiled *in vivo*, before further modifications led to the discovery of **44**  
20  
21 (UCB9608), a vastly more soluble, selective compound with improved metabolic stability and  
22  
23 excellent pharmacokinetic profile. A co-crystal structure of **44** with PI4KIII $\beta$  was solved  
24  
25 confirming the binding mode of this class of inhibitor. The much-improved *in vivo* profile of **44**  
26  
27 positions it as an ideal tool compound, to further establish the link between PI4KIII $\beta$  inhibition  
28  
29 and prolonged allogeneic organ engraftment, and suppression of immune responses *in vivo*.  
30  
31  
32  
33  
34  
35

## 36 INTRODUCTION

37  
38

39 The field of transplantation medicine has seen dramatic advances over the last century with  
40  
41 breakthroughs in management of immune responses and the development of genetically  
42  
43 engineered animals for xenografting, and the emerging use of organs from living donors<sup>1</sup>. In the  
44  
45 United States alone, nearly 17,000 kidney, 6,700 liver, 2,600 heart, and 1,900 lung transplants  
46  
47 are performed annually<sup>2</sup>. Successful management of immunosuppression, heralded by the  
48  
49 discovery that corticosteroids<sup>3</sup> could improve graft retention, led to the key discoveries of the  
50  
51 1980's, which were crucial to the further development of transplantation science. In particular  
52  
53 the discovery of cyclosporine A (CSA)<sup>4</sup> and tacrolimus (Tac or FK506)<sup>5</sup>, cyclic peptides that had  
54  
55  
56  
57  
58  
59  
60

1  
2  
3 profound anti-calcineurin activity, were key. These peptidic calcineurin inhibitors (CNIs) were  
4 found to inhibit T-cell activation resulting in a strong immunosuppressive effect. Current  
5 immunosuppressive regimens promoting long term graft survival use these CNIs in combination  
6 with steroids and myco-phenolate mofetil<sup>6</sup> (MMF). Although reduced allograft rejection rates  
7 have been achieved, there are still risks associated with CNI therapies, including potential  
8 nephrotoxicity<sup>7</sup>, and there remains a case for the discovery of alternative immunosuppressive  
9 agents<sup>8,9</sup> to prevent allograft rejection.



30 **Figure 1:** Previously described 7-Piperazin-1-ylthiazolo[5,4-d]pyrimidin-5-amine analogues with immunosuppressive activity

31  
32 In 2011 Jang et al<sup>10</sup> reported the discovery of a series of novel 7-piperazin-1-ylthiazolo[5,4-  
33 d]pyrimidin-5-amine analogues with a novel immunosuppressive effect (Figure 1). The  
34 compounds were shown to be potent in the human mixed lymphocyte reaction (HuMLR) assay,  
35 often used as a surrogate *in vitro* assay to predict the prevention of rejection *in vivo* of  
36 transplanted organs<sup>11-13</sup>. As well as inhibiting the HuMLR response, **2** appeared to prevent the  
37 rejection of a heterotopic murine cardiac allograft from a C57BL/6 donor mouse to a Balb/C H-2  
38 recipient, confirming that compounds of this class could suppress an allogeneic response *in vivo*.  
39  
40  
41  
42  
43  
44  
45  
46  
47  
48

## 49 RESULTS AND DISCUSSION

50  
51  
52 With **2** as a series exemplar, commercial screening platforms (Cerep<sup>14</sup> and DiscoverX's  
53 KinomeScan<sup>15</sup>) were employed to establish the primary target of these novel inhibitors. No  
54  
55  
56  
57  
58  
59  
60

1  
2  
3 noticeable activity was recorded against the Cerep panel, however kinase profiling suggested the  
4 most likely target of **2** was a member of the lipid kinase family, PI4KIII $\beta$ <sup>16</sup>. PI4KIII $\beta$  is a  
5 phosphatidylinositol kinase widely expressed in mammalian cells, playing an essential role in  
6 membrane trafficking and signal transduction<sup>17</sup>. Sub families include the PI3KC1, C2 and C3  
7 families and the PI4K class II and III's. The PI4K class II's are further divided (PI4KII $\alpha$  and  
8 PI4KII $\beta$ ) as are the PI4K class III's (PI4KIII $\alpha$  and PI4KIII $\beta$ )<sup>18</sup>. PI4K's are essential for the  
9 synthesis of PI4P (phosphatidylinositol 4-phosphate), the most abundant phosphoinositide in  
10 eukaryotic cells<sup>19</sup>, and play critical roles in a number of pathological processes including  
11 mediating the replication of a number of viruses<sup>20</sup>, and in the development of the parasite  
12 responsible for malaria<sup>21</sup>. PI4KIII $\beta$  is also understood to play a key role in cell  
13 compartmentalization, within the Golgi<sup>22</sup> and the trans-Golgi network (TGN). Here it is recruited  
14 by the Golgi resident ACBD3 protein<sup>23</sup>, and plays a role in lysosomal<sup>24</sup> and lipid transport  
15 functions<sup>25</sup>. There is significant interest in targeting PI4KIII $\alpha$  and PI4KIII $\beta$  isoforms as both are  
16 hijacked by multiple viruses which facilitate their entry to target cells and their subsequent  
17 replication<sup>26-29</sup>. At the time of discovery of **2**, there were limited examples of PI4KIII $\beta$  inhibitors  
18 in the literature. PIK93 (**3**, Figure 2), originally developed to target PI3KC1 isoforms<sup>30</sup>, showed  
19 concurrent activity against both PI4KIII $\alpha$  (IC<sub>50</sub> of 1.1  $\mu$ M) and PI4KIII $\beta$  (IC<sub>50</sub> of 0.019  $\mu$ M).  
20 Recently the structure of this pan-lipid kinase, co-crystalized with PI4KIII $\beta$  was published<sup>31,32</sup>.  
21 Furthermore, analogues of PIK-93 such as **4**, have been disclosed with improved PI4KIII $\beta$ <sup>33</sup>  
22 selectivity, with **5**, **6** and **7** emerging as further examples of this class of PI4KIII $\beta$  inhibitor,  
23 showing anti-hepatitis C<sup>34,35</sup> and anti-human rhinovirus<sup>36</sup> activity respectively. The selective  
24 PI4KIII $\beta$  inhibitor **8**, has also been designed to probe the role of phosphatidylinositol signaling in  
25 cancer cell proliferation<sup>37,38</sup>. A somewhat structurally related chemotype exemplified by **9**, was  
26  
27  
28  
29  
30  
31  
32  
33  
34  
35  
36  
37  
38  
39  
40  
41  
42  
43  
44  
45  
46  
47  
48  
49  
50  
51  
52  
53  
54  
55  
56  
57  
58  
59  
60

1  
2  
3 identified as having anti-polio virus activity<sup>39</sup>, and PI4KIII $\beta$  was established as the likely driver  
4 for this observed effect. The synthesis<sup>40</sup> of related analogues such as **10** and the structurally  
5 differentiated **11** have also been disclosed<sup>41</sup> as potent and selective PI4KIII $\beta$  inhibitors with anti-  
6 viral activity established against human rhinovirus and the polio virus. Further core modification  
7 of **9** has also been successful in delivering potent inhibitors of PI4KIII $\beta$ , with excellent  
8 selectivity profiles<sup>42-45</sup>. Rationally designed inhibitors such as **12**, were shown to be broad  
9 spectrum antiviral agents with excellent selectivity for PI4KIII $\beta$  over other lipid kinases, with the  
10 structure of several inhibitors of this type bound to the complex of PI4KIII $\beta$ /wtRab11 disclosed.  
11  
12  
13  
14  
15  
16  
17  
18  
19  
20  
21  
22

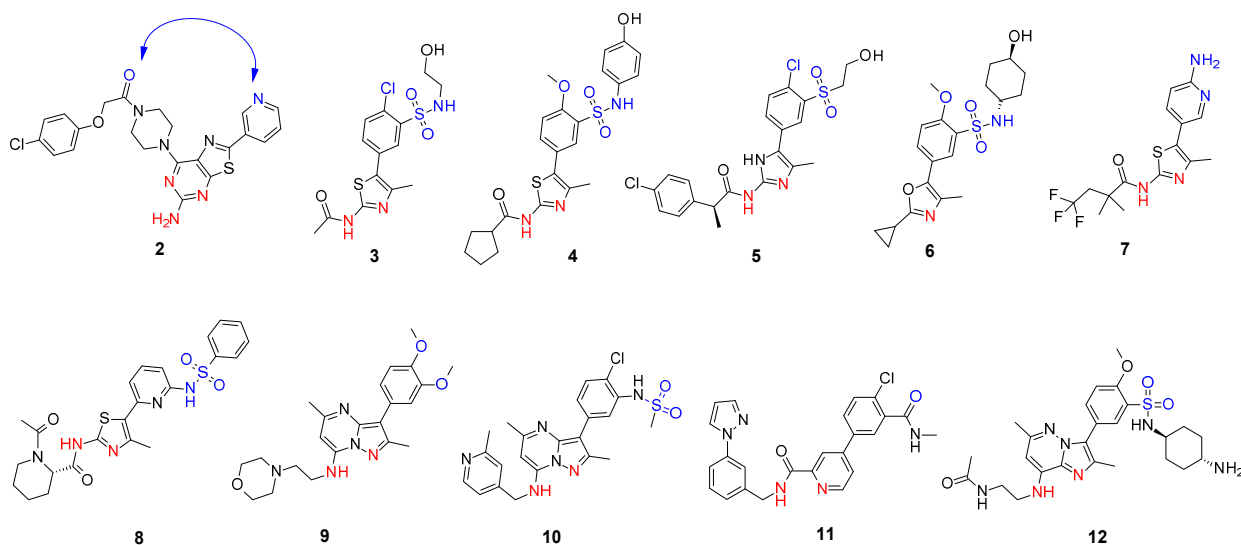


**Figure 2.** Compound **2** in a proposed alignment with exemplar structures of PI4KIII $\beta$  inhibitors from literature (**3-12**). The nitrogen atoms postulated to form the key mono or bi-dentate interaction with the kinase hinge region are shown in red. Atoms in blue, are likely to be involved in a second critical interaction with the catalytic lysine residue of PI4KIII $\beta$ . It was plausible **2** could adopt multiple binding modes with the piperazine and 3-pyridyl groups ‘flipping’ to make a putative interaction with the lysine residue (as highlighted by the blue arrow).

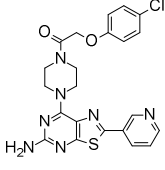
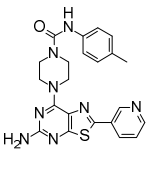
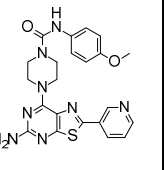
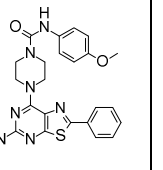
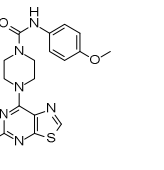
Compounds (**2-12**) all share a putative hydrogen bonding interaction with the hinge region of PI4KIII $\beta$ . A second interaction to a catalytic lysine is also present in compounds **3-12**, however it was not clear if **2** was deriving its activity by making the same interaction (Figure 2). To this end, we sought to confirm the binding mode of these novel inhibitors, establish the link between PI4KIII $\beta$  inhibition and impaired immune cell function, and evaluate if PI4KIII $\beta$  inhibitors from

1  
2  
3 this unique series had the potential to become part of a new CNI sparing immunosuppressive  
4 regimen for the prevention of the rejection of solid organ allografts. The HuMLR continued to be  
5 used in the absence of any cellular assay where PI4KIII $\beta$  target engagement could be directly  
6 measured. As discussed previously, the HuMLR is a phenotypic assay, and used as a predictor of  
7 the classical immune response (i.e. ‘self’ responding to ‘non-self’). To validate the effectiveness  
8 of the HuMLR as a surrogate cellular assay for assessing PI4KIII $\beta$  inhibitors as  
9 immunosuppressive agents, the IC<sub>50</sub>'s of a selection of differentiated PI4KIII $\beta$  chemotypes from  
10 Figure 2 were generated. PIK-93 (**3**) was found to inhibit the HuMLR with an IC<sub>50</sub> of 28 nM,  
11 however as discussed previously, PIK-93 is a pan-lipid kinase inhibitor, designed to primarily  
12 target the PI3K's. The more selective analogue **5** was also found to inhibit the HuMLR, with an  
13 IC<sub>50</sub> of 71 nM, in line with its reported PI4KIII $\beta$  activity<sup>46</sup>. Compound **9** showed modest activity  
14 in the HuMLR (IC<sub>50</sub> of 2  $\mu$ M), likely due to its poor cell permeability, whilst **10** inhibited the  
15 HuMLR with an IC<sub>50</sub> of 8 nM. Finally, **11** was found to have an IC<sub>50</sub> against the HuMLR of 18  
16 nM. Both **10** and **11** were described as being selective inhibitors of PI4KIII $\beta$  kinase<sup>47</sup>, adding  
17 weight to the notion that PI4KIII $\beta$  inhibition was responsible for the reduced HuMLR response  
18 of this structurally diverse set of inhibitors (**2**, **5**, **10** and **11**). As a means of prioritizing  
19 compounds for evaluation as potential immunosuppressive agents *in vivo*, the HuMLR was  
20 deemed to be a simplistic and robust assay to continue to screen against, although whether all  
21 PI4KIII $\beta$  inhibitor chemotypes could replicate the effect seen with compound **2** *in vivo*, remained  
22 to be confirmed. A more in-depth evaluation of analogues of **1** and **2**, some of which were  
23 detailed in the previous KUL publication<sup>10</sup>, was now undertaken at UCB. This included *in vitro*  
24 safety profiling (drug-drug interaction (DDI) risk and cardiovascular safety (CVS) risk), *in vitro*  
25 metabolic stability in Mouse Liver Microsomes (MLM) and Human Liver Microsomes (HLM)



and measurement of physico-chemical parameters such as LogD and solubility. Of the many compounds profiled, **2** and **13** stood out as potent examples of amide and urea capped 7-piperazin-1-ylthiazolo[5,4-*d*]pyrimidin-5-amine analogues respectively (Table 1).

**Table 1:** Early in vitro profiling of 7-piperazin-1-ylthiazolo[5,4-*d*]pyrimidin-5-amine series

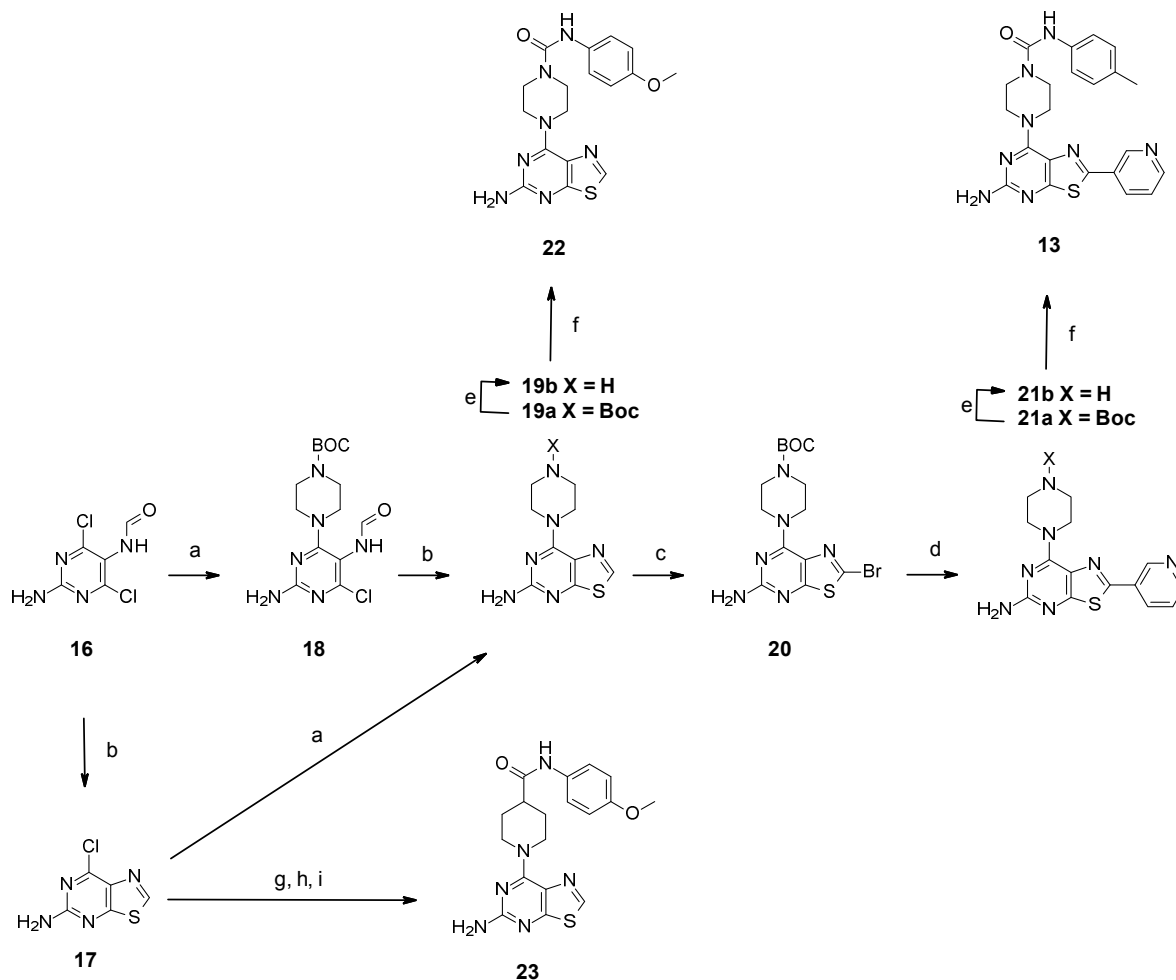
| Compound:   | <b>2</b>  | <b>13</b>   | <b>14</b>  | <b>15</b>   | <b>22</b>   |
|---|---|---|--|---|---|
|   |  |  |  |  |  |
| PI4KIIIβ IC <sub>50</sub> (nM) <sup>a</sup>                     | <b>10</b>   | <b>19</b>   | <b>2</b>   | <b>11</b>   | <b>51</b>   |
| Hu MLR IC <sub>50</sub> (nM) <sup>a</sup>                       | <b>16</b>   | <b>5</b>  | <b>4</b>   | <b>32</b>   | <b>53</b>   |
| MLM CL <sub>int</sub> (μl.min <sup>-1</sup> .mg <sup>-1</sup> ) | <b>133</b>  | <b>72</b>   | <b>87</b>  | <b>20</b>   | <b>15</b>   |
| HLM CL <sub>int</sub> (μl.min <sup>-1</sup> .mg <sup>-1</sup> ) | <b>34</b>   | <b>32</b>   | <b>35</b>  | <b>13</b>   | <b>21</b>   |
| hERG IC <sub>50</sub> (μM)                                      | - <sup>c</sup>  | <b>2.0</b>  | <b>2.2</b>   | <b>1.7</b>  | <b>28</b>   |
| CYP3A4 IC <sub>50</sub> (μM)                                    | - <sup>c</sup>  | <b>0.9</b>  | <b>1.6</b>   | <b>&gt;20<sup>c</sup></b>   | <b>&gt;20</b>   |
| LogD (pH7.4)  | - <sup>c</sup>  | <b>3.42</b>   | <b>3.06</b>  | - <sup>c</sup>  | <b>1.85</b>   |
| Solubility (μM) <sup>b</sup>                                    | - <sup>c</sup>  | <b>9</b>  | <b>32</b>  | <b>6</b>  | <b>85</b>   |

<sup>a</sup> IC<sub>50</sub> values are reported as means of values from at least 2 determinations. <sup>b</sup> Kinetic solubility measured from 10mM DMSO stock at pH<sub>7.4</sub>. <sup>c</sup> Poor solubility means data was unobtainable or should be treated with caution.

Although both compounds showed promising potency, the solubility of **2** and **13** was poor, and CL<sub>int</sub> in HLM and MLM moderate to high. Compound **13** was also found to inhibit the hERG channel with an IC<sub>50</sub> of 2 μM (automated patch-clamping (Q-Patch)), indicative of a potential CVS risk<sup>48</sup> as well as CYP3A4, with an IC<sub>50</sub> of 0.9 μM, indicative of a potential DDI risk<sup>49</sup>. It was not possible to profile **2** in these assays due to its poor solubility. Urea analogue **14**, showed improved PI4KIIIβ and HuMLR potency, but remained a strong inhibitor of both hERG and CYP3A4, with CL<sub>int</sub> in HLM and MLM remaining high. The phenyl analogue, **15** maintained acceptable activity suggesting the 3-pyridyl nitrogen in **14** was not critical for maintaining

PI4KIII $\beta$  activity. Encouragingly **15** appeared to be more stable (compared to **14**) in HLM and MLM, whilst CYP3A4 inhibition appeared significantly reduced, although it is noted that the poor solubility of this compound meant that this data should be treated with caution.

### Scheme 1. Synthesis of compounds **13**, **22** and **23**



Reagents and conditions: (a) Boc-Piperazine, 1,4 dioxane, DIPEA, 1 h, 55 °C, quant.; (b) Lawesson's reagent, 1,4 dioxane, 0.5 h, 65 °C, 93%; (c) NBS, DMF, 3 h, 55%; (d) 3-(Et<sub>2</sub>B)-Pyridine, Na<sub>2</sub>CO<sub>3</sub> (aq), Pd(0)(PPh<sub>3</sub>)<sub>4</sub>, DME, 150°C, CEM microwave, 0.5 h, 45%; (e) 4N HCl in 1,4 dioxane, DCM, 1-16 h, 72-100%; (f) Isocyanate, DIPEA or Et<sub>3</sub>N, DCM or DMF, 4 h, 20-95%; (g) Ethyl Isonipecotate, DIPEA, 1,4-dioxane, 12 h, 70°C 50%; (h) 10% NaOH, THF/MeOH (5:1), 6 h, quant; (i) *p*-Anisidine, HOBT.H<sub>2</sub>O, EDCI, DIPEA 14 h, 81%.

It could not be ruled out that removal of the pyridyl nitrogen, a potential heme binding element could be playing a significant part in the improved *in vitro* ADME profile observed with **15**. The

1  
2  
3 route previously<sup>10</sup> utilized to access compounds **2** and **13** was modified to allow for exploration  
4  
5 of the 2-position of the thiazolo[5,4-*d*]pyrimidine-5-amine core. The *boc*-protected 2*H*-  
6  
7 thiazolo[5,4-*d*]pyrimidine-5-amine **19a** was synthesized from commercial **16** in 2  
8  
9 interchangeable steps according to Scheme 1. Bromination of intermediate **19a** using NBS in  
10  
11 1,4-dioxane yielded **20**, a flexible intermediate suitable for the exploration of the 2-position via a  
12  
13 range of coupling methodologies. To validate the route, compound **13** was re-synthesized using  
14  
15 this new approach, coupling diethyl(3-pyridyl) borane with **20**. Deprotection of **21a** then  
16  
17 subsequent capping with commercial 4-methylphenyl isocyanate gave **13** in good yields. It was  
18  
19 intended that with **20** in hand, a SAR exploration of the 2-position could be initiated with the aim  
20  
21 of identifying potent, soluble and more metabolically stable analogues of **14** and **15** that were  
22  
23 free of hERG and CYP liabilities. Interestingly, upon testing the unsubstituted 2*H*-thiazolo[5,4-  
24  
25 *d*]pyrimidine-5-amine analogue **22**, an acceptable level of PI4KIII $\beta$  and HuMLR activity could  
26  
27 be maintained. Indeed, with this ring excised, LogD was reduced, and subsequently MLM and  
28  
29 HLM CL<sub>int</sub> were improved. A modest improvement in kinetic solubility was also noted, and both  
30  
31 CYP3A4 and hERG inhibition (although not completely ablated), were much reduced (Table 1).  
32  
33 At this juncture, both **13** and **22** were chosen for kinase selectivity profiling. A set of 250  
34  
35 diverse kinases<sup>50</sup> were screened at a concentration of 10  $\mu$ M. No activity was noted against any  
36  
37 tested kinase aside from a handful of lipid kinase isoforms. Concentration responses (IC<sub>50</sub>) were  
38  
39 obtained against the 12 available lipid kinases<sup>51</sup>, and a selectivity profile for **13** and **22** generated  
40  
41 (Figure 3). It appeared **22** was 15-fold selective for PI4KIII $\beta$  over PI3KC2 $\gamma$ <sup>52</sup>, 50-fold over  
42  
43 PI3KC2 $\alpha$  and 120-fold over PI3KC2 $\beta$ . Compound **13**, with the appended 3-pyridyl ring,  
44  
45 appeared to be more selective for PI4KIII $\beta$  over the PI3KC2 family of kinases in comparison.  
46  
47 The impact of this modest PI3KC2 inhibition was not clear, as the role of these kinases in  
48  
49  
50  
51  
52  
53  
54  
55  
56  
57  
58  
59  
60

disease, and their subsequent utility as therapeutic targets<sup>53</sup> is still being explored. Encouragingly, both **13** and **22** showed no activity against the other PI4K isoforms, and maintained good selectivity (>100 fold) over the class 1 PI3K  $\alpha$ ,  $\beta$ ,  $\gamma$  and  $\delta$  isoforms (Figure 3).

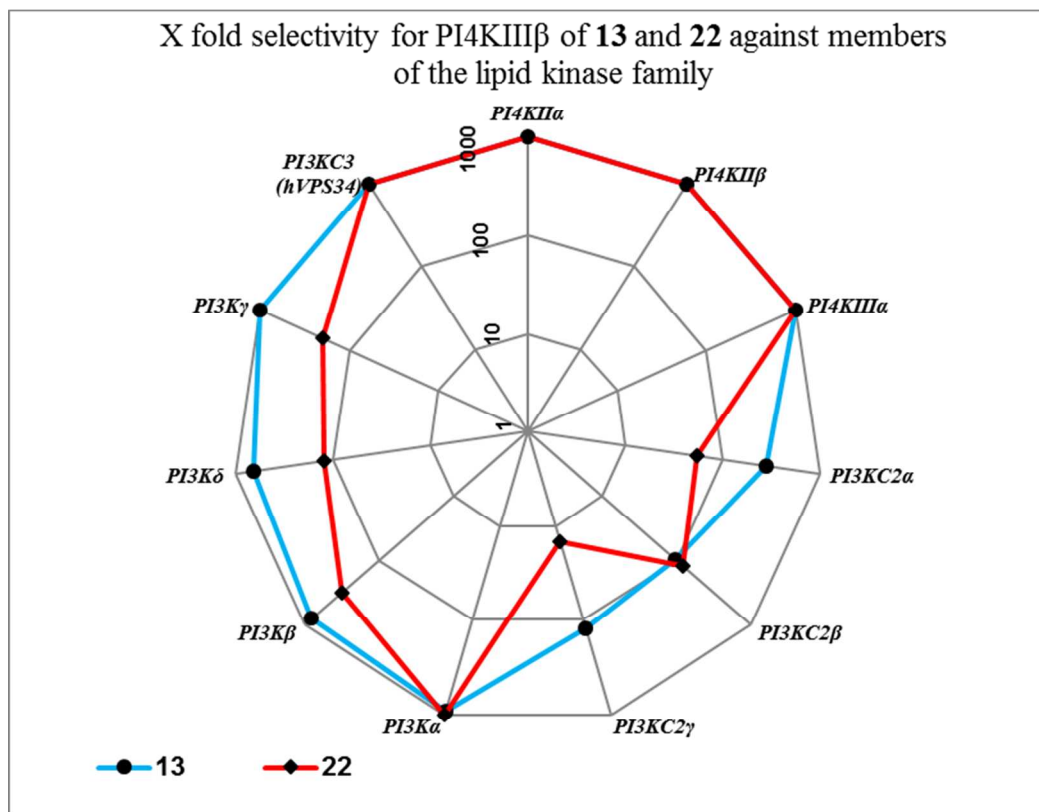


**Figure 3.** Radial plot of lipid kinase selectivity of **13** and **22** for PI4KIII $\beta$  over the other 11 lipid kinase family members tested.

Compound **22** was chosen based on its *in vitro* profile to evaluate PI4KIII $\beta$  inhibition in murine models of T-cell mediated immune response. The blood concentration vs time profile in male Balb/C mice following oral administration at 10, 30 and 100 mpk was determined for **22**, prior to evaluation in a mouse model of anti-CD3 mediated T-Cell activation<sup>54</sup>. Exposure appeared to increase in proportion to dose, however there was significant inter-individual variation in exposure observed, likely influenced by the poor solubility of **22** leading to highly variable oral

absorption across the doses tested.  $C_{max}$  (free) was achieved at around 1h at all doses, and for the 100 mpk dose, was between 10 and 30-fold over the HuMLR  $IC_{50}$ .

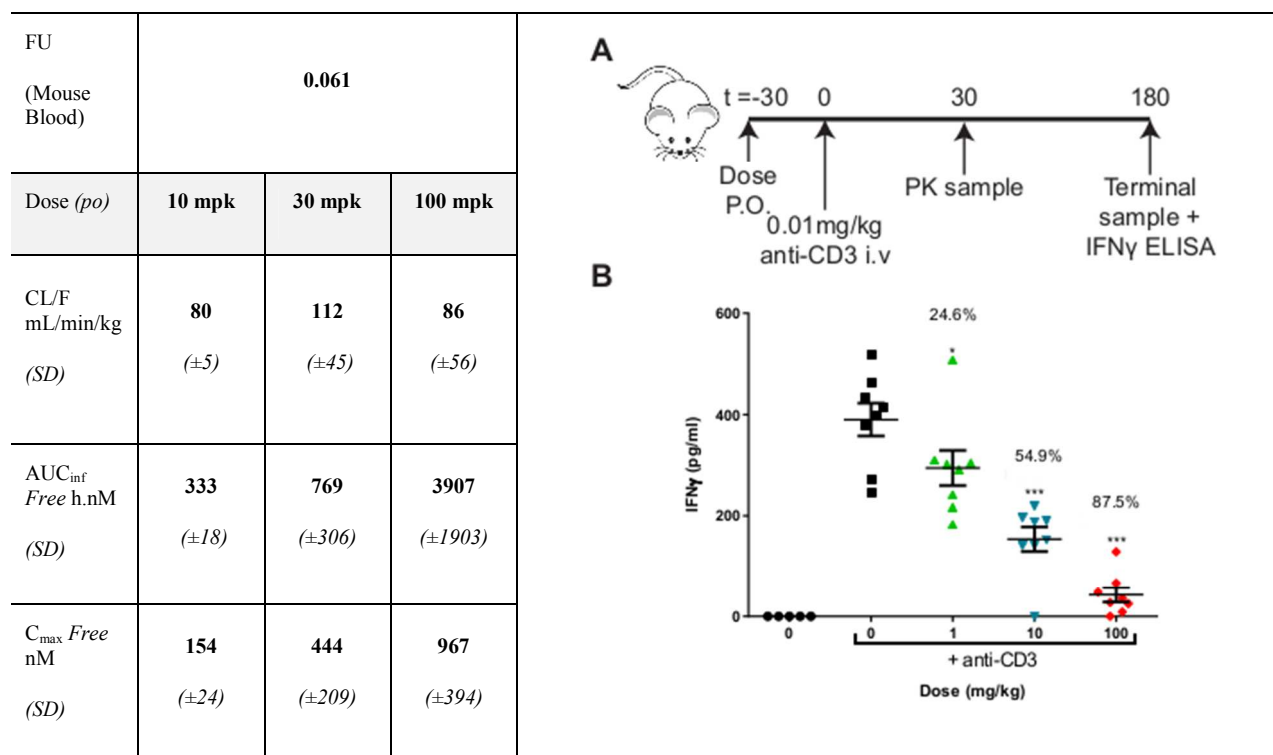


**Figure 4.** Oral PK parameters were determined in male Balb/C mice,  $n=3$ , at the specified dose, with crystalline **22** given as a homogeneous suspension in vehicle (0.1 % (w/v) Tween 80, 0.1 % (w/v) Silicone antifoam in 1 % (w/v) methylcellulose (400 cps) in water). (A) Time course (in minutes) for assessing the inhibition of anti-CD3 induced T-Cell activation of  $IFN\gamma$  release by **22**. (B) Measured levels of  $IFN\gamma$  release (pg/ml) for negative control, +ve control (vehicle (0.1 % (w/v) Tween 80, 0.1 % (w/v) Silicone antifoam in 1 % (w/v) methylcellulose (400 cps) in water)), 1, 10 and 100mpk of **22** (all groups  $n=8$ ). % Inhibitions refer to the mean ( $\pm$  SEM). \* $P<0.05$  Compared to +ve control by Dunnetts multiple comparison test. \*\*\* $P<0.001$  compared to +ve control by Dunnetts multiple comparison test. PK samples were taken 1h after dosing with **22** to coincide with  $C_{max}$  and confirmed exposures achieved in the experiment were in line with those achieved during the PK study.

As seen in Figure 4, **22** significantly inhibited  $IFN\gamma$  release compared to vehicle treated animals in a dose dependent manor, indicative of **22** having a strong inhibitory effect on T-Cell activation. Subsequent evaluation of **22** in a longer term oxazolone (OXA) induced T-cell dependent model of antibody response<sup>55</sup> (Figure 5) showed that **22** could also significantly inhibit IgG1 production at a dose of 100 mpk (PO). With **22** able to inhibit a range of T-cell mediated antibody responses *in vivo*, it was left to evaluate if the modified urea **22** remained

efficacious in the murine model of cardiac allograft rejection<sup>10</sup> previously described by the team at KUL. Balb/C mice carrying a heterotopically transplanted heart from a C57B6 donor were treated once daily with 100 mpk of **22**, and long term graft survival rates of ~50%, when compared to vehicle<sup>56</sup> alone, could be achieved. Significantly animals treated with **22** continued to maintain their grafts after treatment withdrawal, differentiating them from CSA treated animals (Figure 5) where rejection occurred days after treatment withdrawal.

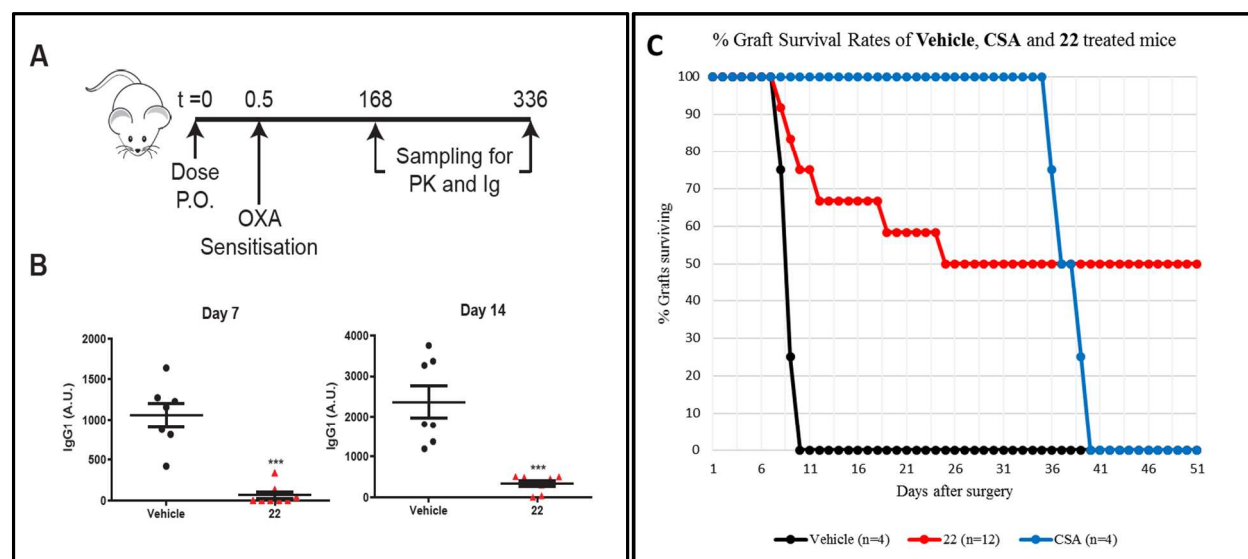
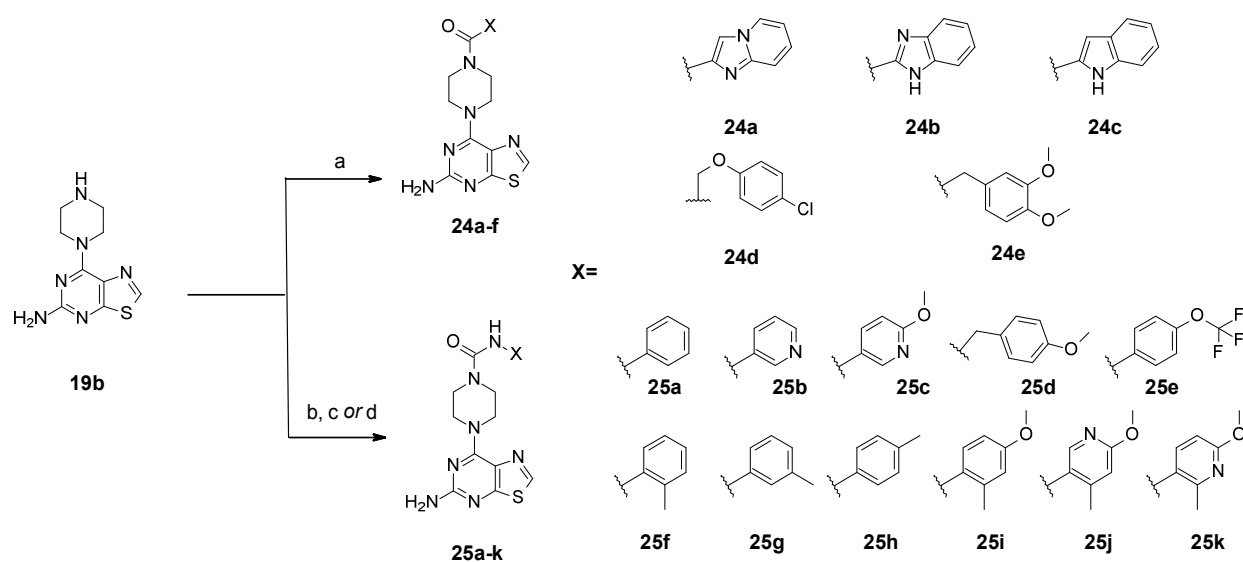


**Figure 5.** (A) Time course (in hours) for assessing the inhibition of OXA induced IgG1 release by **22** (n=8). (B) Measured IgG1 levels after daily dosing of vehicle (0.1 % (w/v) Tween 80, 0.1 % (w/v) Silicone antifoam in 1 % (w/v) methylcellulose (400 cps) in water) and **22** (100 mpk of crystalline **22** as a homogeneous suspension in vehicle), measured at day 7 and day 14 compared to vehicle control (arbitrary units (A.U.)). \*\*\*P<0.001 Compared to +ve control by Dunnetts multiple comparison test. (C) Comparison of survival rates for engrafted mice treated with vehicle (0.1 % (w/v) Tween 80, 0.1 % (w/v) Silicone antifoam in 1 % (w/v) methylcellulose (400 cps) in water), CSA (40 mpk as a solution in vehicle) and **22** (100 mpk of crystalline **22** as a homogeneous suspension in vehicle). Animals were dosed via oral gavage once a day for 28 days, or until a transplanted graft had ceased beating, indicative of rejection. Graft survival is defined as a strongly beating heart (as confirmed by visual inspection and palpitation).

The majority of graft rejection seen with **22** took place during a time critical period post-surgery, when risk of acute rejection is at its highest<sup>57</sup>. Given the delicate nature of the surgery involved, obtaining multiple PK samples during this critical time was challenging, and establishing the relationship between free drug levels and long-term graft survival was problematical. With the high inter-individual variability in exposure following oral administration of **22**, possibly driven by poor solubility (see Figure 4), there remained uncertainty as to how much drug each engrafted

1  
2  
3 animal was receiving, during the critical post-surgery window. To establish more accurately the  
4 link between PI4KIII $\beta$  inhibition and successful engraftment in this, and other transplantation  
5 models, a tool compound from this series, with a much improved and reproducible PK profile  
6 was required. Further SAR exploration was undertaken to improve potency and solubility whilst  
7 establishing if compounds such as **22**, carrying an embedded electron rich anilino-urea, posed  
8 any toxicity liability. Many aryl urea's are found in marketed kinase inhibitors<sup>58</sup>, but there  
9 remains a potential for the metabolically triggered release of electron rich anilines, raising a  
10 potential genotoxicity<sup>59</sup> or liver toxicity risk, as seen with acetaminophen<sup>60</sup>. Considerable effort  
11 was spent seeking more soluble, non-urea equivalents of **22**. Firstly, the piperidine amide  
12 equivalent **23**, was made as detailed in Scheme 1.

### 27 Scheme 2: Synthesis of amide, aryl and heteroaryl urea analogues of **22**

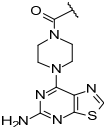
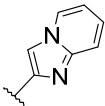
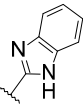
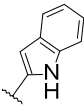
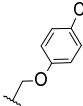
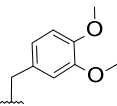


Reagents and conditions: (a) Acid, HATU, DIPEA, DMF, 12 h, 50-90%; (b) Aryl-isocyanate, DIPEA or Et<sub>3</sub>N, DCM or DMF, 4 h, 20-95%; (c) Aryl-amine, CDI, DMF, DIPEA, 4 h, 20-95%; (d) Aryl-amine, PhOCOCl, pyridine, THF then DIPEA, DMSO 3 h 60°C 50 and 90%.

51 Swapping out the piperazine urea nitrogen for an *SP*<sup>3</sup> carbon was significantly detrimental to  
52 PI4KIII $\beta$  activity (IC<sub>50</sub> >6  $\mu$ M). Subsequently focus turned to making piperazine amides.  
53  
54  
55  
56  
57  
58  
59  
60

Libraries of aliphatic and aromatic amides were made, however all but a few showed potencies in the sub- $\mu\text{M}$  range, with the synthesis of key examples detailed in Scheme 2. These included heterocyclic amides such as the imidazo-pyridine **24a**, that also showed a modest improvement in solubility. Attempts to improve potency by adding back the hydrogen bond donor of **22**, were unsuccessful, with benzimidazole **24b** and indole **24c** significantly less active (Table 2). The only amide analogue of **22** that appeared to have any significant potency was **24d**, an analogue of the original lead **2**. The  $\text{IC}_{50}$  against PI4KIII $\beta$  was 216 nM but solubility was significantly worse than **22**, with subsequent analogues continuing to suffer from modest potency, poor solubility and metabolic instability. The phenyl acetamide **24e**, where the NH of **22** is swapped for a methylene, was significantly less active, adding to the evidence supporting the importance of the urea CO and NH in maintaining activity.

**Table 2: SAR of non-urea analogues of 22**

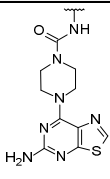
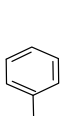
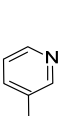
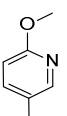
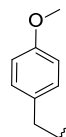
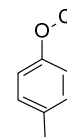
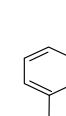
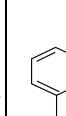
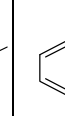
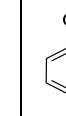
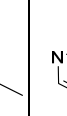
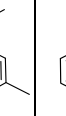
| Cpd   | <b>24a</b>  | <b>24b</b>  | <b>24c</b>   | <b>24d</b>  | <b>24e</b>  |
|---|---|---|--|---|---|
|  |  |  |  |  |  |
| PI4KIII $\beta$ $\text{IC}_{50}$ (nM) <sup>a</sup>                                  | <b>946</b>  | <b>6138</b>   | <b>&gt;10000</b>   | <b>216</b>  | <b>5743</b>   |
| HuMLR $\text{IC}_{50}$ (nM) <sup>a</sup>  | <b>8795</b>   | <b>&gt;10000</b>  | <b>&gt;10000</b>   | <b>635</b>  | <b>&gt;10000</b>  |
| LogD (pH7.4)  | <b>1.58</b>   | <b>2.54</b>   | <b>2.84</b>  | <b>2.68</b>   | <b>1.50</b>   |
| Solubility <sup>b</sup> ( $\mu\text{M}$ )   | <b>&gt;350</b>  | <b>38</b>   | <b>14</b>  | <b>13</b>   | <b>&gt;350</b>  |

<sup>a</sup>  $\text{IC}_{50}$  values are reported as means of values from at least 2 determinations. <sup>b</sup> Kinetic solubility measured from DMSO stock at pH<sub>7.4</sub>

Without a published PI4KIII $\beta$  crystal structure (*at this time*) to aid design, further efforts to seek urea replacements were halted. The concern around the inherent risk of genotoxicity associated with embedded electron rich anilines prompted the profiling of **22** in a 3 strain bacterial mini-AMES<sup>61</sup> test. It concluded that **22** was non-mutagenic at the top concentrations tested, with and



without metabolic activation. There was however literature evidence to suggest 4-methoxy aniline (*p*-anisidine) was a likely genotoxic liability<sup>62</sup>, although metabolite profiling of **22** concluded no liberation of 4-methoxy aniline in the presence of isolated human liver microsomes<sup>63</sup>. A wide range of alternative urea analogues were synthesized to explore SAR, drive potency and improve solubility, with key examples detailed in Table 3. Unsubstituted aniline urea **25a** was significantly less active, as was the 3-pyridyl urea, **25b**, although kinetic solubility was improved. Potency could be returned to **25b**, by making the methoxy-pyridine analogue **25c**, which maintained modest potency, although 10-fold less active than **22**. Homologation to the benzyl urea **25d** reduced activity, with the more electron-withdrawing 4-OCF<sub>3</sub> analogue, **25e** 10-fold less active than **22**. A simple methyl scan of the aryl urea (**25f-h**) showed a slight preference for *ortho* or *para* substitution over *meta*, with all three compounds appearing less active than **22**, and significantly less soluble.

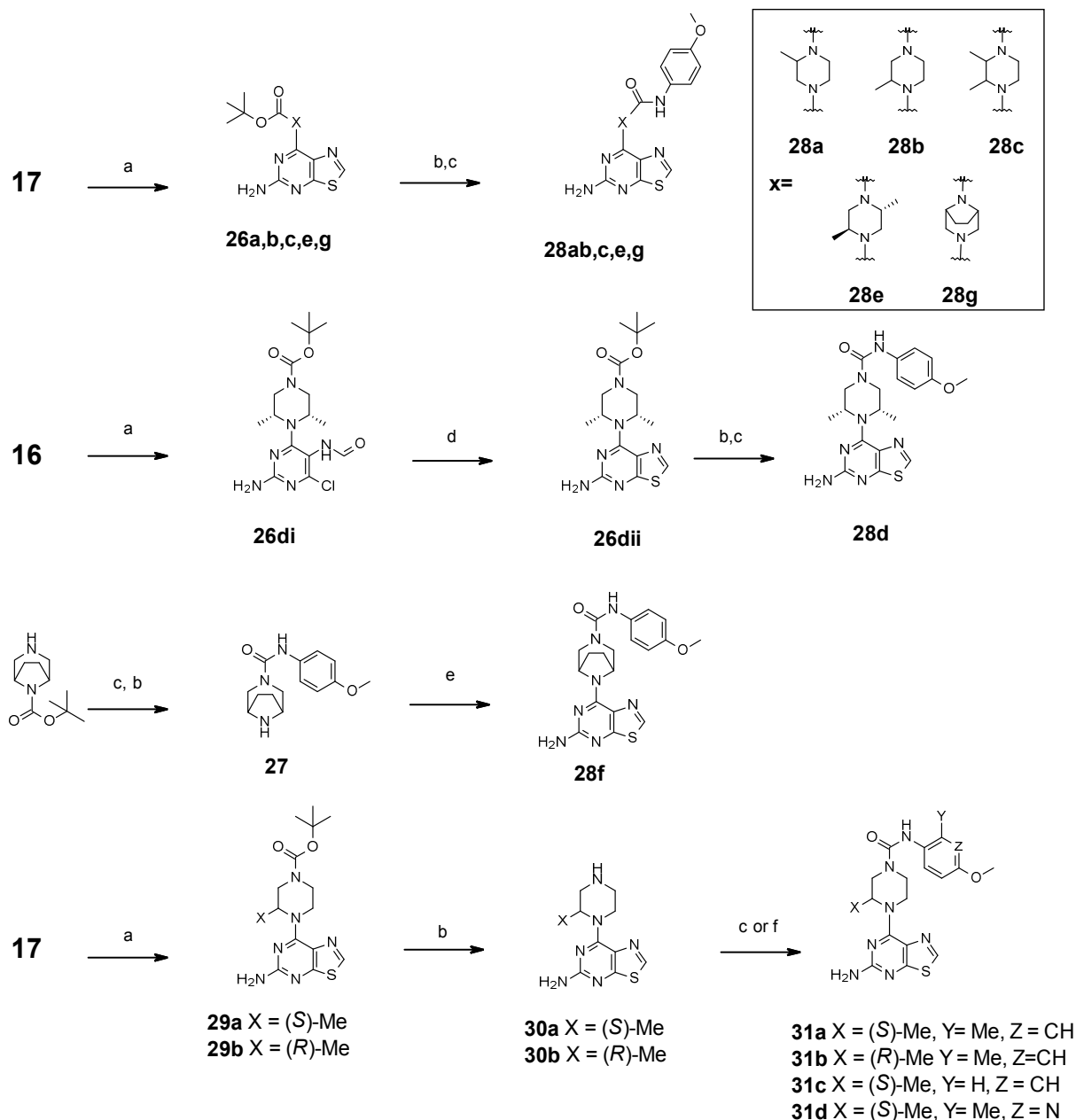
| Cpd   | <b>25a</b>  | <b>25b</b>  | <b>25c</b>  | <b>25d</b>  | <b>25e</b>  | <b>25f</b>  | <b>25g</b>  | <b>25h</b>  | <b>25i</b>  | <b>25j</b>  | <b>25k</b>  |
|---|---|---|---|---|---|---|---|---|---|---|---|
|  |  |  |  |  |  |  |  |  |  |  |  |
| PI4KIIIβ IC <sub>50</sub> (nM) <sup>#</sup>   | 517   | 3387  | 611   | 1946  | 548   | 114   | 312   | 145   | 9   | 414   | 173   |
| Hu MLR IC <sub>50</sub> (nM) <sup>a</sup>   | 380   | >5000   | 424   | 1764  | 331   | 150   | 115   | 85  | 35  | 656   | 195   |
| Solubility (μM) <sup>b</sup>  | 178   | >350  | 293   | 33  | 12  | 33  | 34  | 21  | 33  | >350  | 207   |
| LogD (pH 7.4)   | 2.21  | 1.46  | 1.79  | 2.22  | 3.39  | 2.12  | 2.81  | 2.55  | 2.03  | 1.66  | 1.65  |

**Table 3: SAR of aryl and heteroaryl urea analogues of **22****

<sup>a</sup> IC<sub>50</sub> values are reported as means of values from at least 2 determinations. <sup>b</sup> Kinetic solubility measured from DMSO stock at pH<sub>7.4</sub>

1  
2  
3 The observation that an ortho-methyl group was tolerated in **25f**, was exploited and **25i** the 2-  
4 methyl-4-methoxy anilino urea found to have an IC<sub>50</sub> of 9 nM against PI4KIIIβ, with activity  
5 maintained in the HuMLR. Solubility however was poor, although could again be improved by  
6 making pyridine analogues **25j** and **25k**. Again however, this came at the cost of potency, with  
7 **25k** the most active, with an IC<sub>50</sub> of ~200 nM in the HuMLR. Further efforts to solubilize **25i**  
8 through aryl substitution, aryl ring modification or addition of solubilizing groups to the critical  
9 methyl or methoxy substituents (data not shown) failed to give the balance of potency and  
10 solubility required. Focus next shifted to reducing the planar nature of the compounds by  
11 inducing a twist to the piperazine linker. It is known that by reducing ‘flatness’ or through the  
12 introduction of more 3-dimensional structure, the solubility of drug like molecules<sup>64</sup> can be  
13 significantly improved. Thus, a broad range of mono-protected substituted piperazines were  
14 identified with the synthesis of key analogues of **22**, detailed in Scheme 3. When a methyl was  
15 introduced adjacent to the urea linker (**28a**), solubility was enhanced, but potency impacted.  
16 When the methyl was added adjacent to the piperazine nitrogen linking to the hinge binding  
17 group (**28b**), both primary and cellular potency as well as kinetic solubility were much improved  
18 relative to **22**. A further set of di-methylated and bridged piperazine linkers were synthesized  
19 (**28c-28g**), although none combined the potency and solubility improvements seen with **28b**  
20 (Table 4). Through use of the respective chiral boc-methyl piperazines, building blocks **30a** and  
21 **30b** were synthesized to establish if there was any enantiomeric preference. Capping was then  
22 undertaken with the most potent urea to date, derived from 2-methyl-4-methoxy aniline. As can  
23 be seen in Table 4, there was a clear preference for the (*S*) enantiomer over the (*R*) with **31a**  
24 becoming the most potent analogue of **22** made to date.  
25  
26  
27  
28  
29  
30  
31  
32  
33  
34  
35  
36  
37  
38  
39  
40  
41  
42  
43  
44  
45  
46  
47  
48  
49  
50  
51  
52  
53  
54  
55  
56  
57  
58  
59  
60

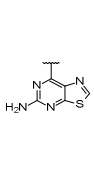
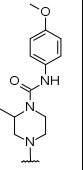
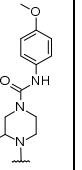
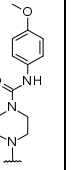
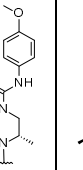
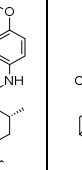
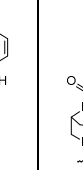
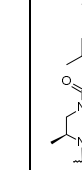
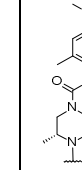
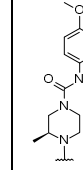
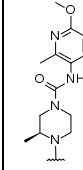

## Scheme 3: Synthesis of substituted piperazine analogues



Reagents and conditions: (a) Substituted Boc-piperazine, DIPEA, 1,4-dioxane 55-100 °C 12-100h, 6-80%; (b) TFA or HCl in 1,4-dioxane, rt 2-24 h, 80-100%; (c) Isocyanate, DIPEA, DCM or DMF, rt 10-24h, 40-80%, (d) Lawesson's reagent, THF, 70°C, 3h, quant.; (e) Intermediate **17**, DIPEA, 1,4-dioxane, 100 °C, 100h, 20%; (f) 6-MeO-2-Me-pyridin-3-amine, phenyl chloroformate, Pyridine, THF 0°C then addition to **30b** in DMSO with DIPEA, 60°C, 3h 55%.

Although **31a** appeared to show a modest improvement in kinetic solubility, when thermodynamic solubility<sup>65</sup> was measured there was no apparent difference in the solubility of **22** and **31a**. The direct analogue of **22**, bearing a single chiral methyl on the piperazine, **31c** was made, and single digit nM potency maintained with improved thermodynamic solubility compared to **22**.

**Table 4: SAR of substituted piperazine urea analogues**

| Cpd   | <b>28a</b>  | <b>28b</b>  | <b>28c</b>  | <b>28d</b>  | <b>28e</b>  | <b>28f</b>  | <b>28g</b>   | <b>31a</b>  | <b>31b</b>  | <b>31c</b>  | <b>31d</b>  |
|---|---|---|---|---|---|---|--|---|---|---|---|
|  |  |  |  |  |  |  |  |  |  |  |  |
| PI4KIIIβ<br>IC <sub>50</sub><br>(nM) <sup>a</sup>                                 | <b>1500</b>   | <b>18</b>   | <b>2583</b>   | <b>1412</b>   | <b>275</b>  | <b>981</b>  | <b>2577</b>  | <b>4</b>  | <b>316</b>  | <b>8</b>  | <b>20</b>   |
| Hu MLR<br>IC <sub>50</sub><br>(nM) <sup>a</sup>                                   | <b>&gt;10000</b>  | <b>23</b>   | <b>2712</b>   | <b>543</b>  | <b>381</b>  | <b>635</b>  | <b>1768</b>  | <b>8</b>  | <b>472</b>  | <b>31</b>   | <b>60</b>   |
| Kinetic<br>Solubility<br>(μM) <sup>b</sup>  | <b>&gt;350</b>  | <b>&gt;350</b>  | <b>&gt;350</b>  | <b>83</b>   | <b>88</b>   | <b>&gt;350</b>  | <b>&gt;350</b>   | <b>160</b>  | <b>170</b>  | <b>&gt;350</b>  | <b>&gt;350</b>  |
| Solubility<br>-TD<br>(μM) <sup>c</sup>  | -   | -   | -   | -   | -   | -   | -  | <b>3</b>  | -   | <b>30</b>   | <b>362</b>  |
| hERG<br>IC <sub>50</sub> (μM)   | -   | -   | -   | -   | -   | -   | -  | -   | -   | <b>17</b>   | <b>&gt;30</b>   |
| CYP3A4<br>IC <sub>50</sub> (μM)   | -   | -   | -   | -   | -   | -   | -  | <b>&gt;20<sup>d</sup></b>   | -   | <b>&gt;20</b>   | <b>&gt;20</b>   |

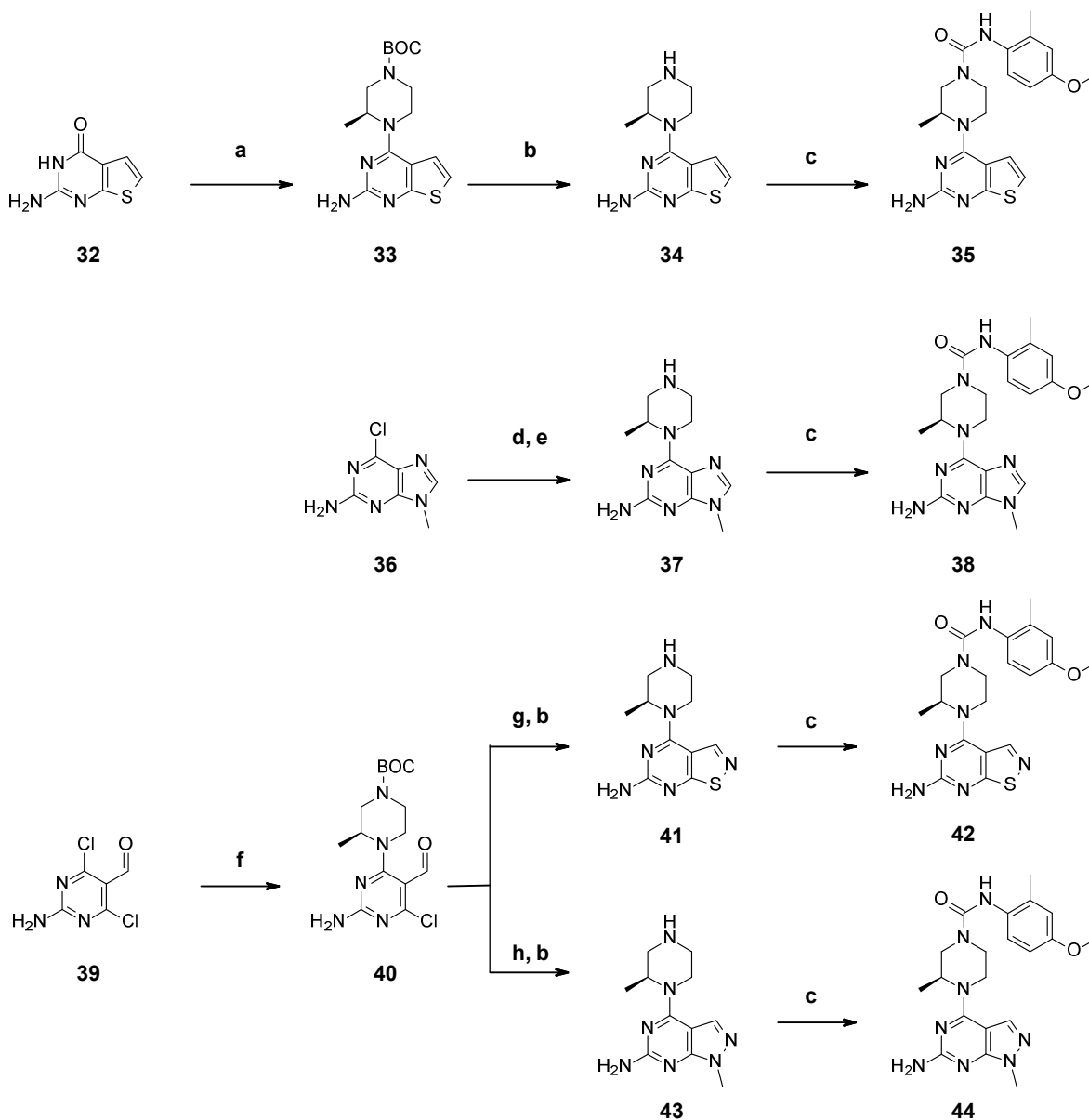
<sup>a</sup>IC<sub>50</sub> values are reported as means of values from at least 2 determinations. <sup>b</sup>Kinetic solubility measured from DMSO stock at pH<sub>7.4</sub>.

<sup>c</sup>Thermodynamic solubility (TD) measured from solid stock at pH<sub>7.4</sub>. <sup>d</sup>Figure should be treated with caution due to low solubility.

The pyridyl analogue **31d** showed a 5-fold drop off in PI4KIIIβ activity, but was still more potent than **22** and exhibited excellent thermodynamic solubility. There was no CYP3A4 inhibition observed with any (*S*) methyl piperazine analogue tested, and pyridyl urea **31d** was

clean in hERG. The more lipophilic **31c** however did exhibit a stronger hERG signal than **22**, but not enough to warrant concerns at this stage.

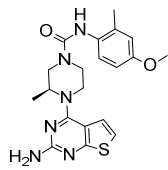
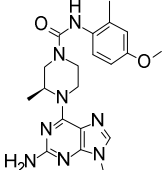
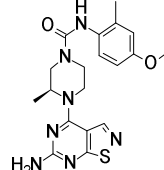
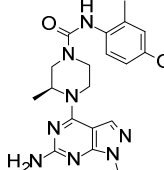
#### Scheme 4: Synthesis of hinge binder analogues of **31a**



Reagents and conditions: (a) PyBOP, DBU, acetonitrile, Boc-piperazine 60 °C 72 h, 66%; (b) 4N HCl in 1,4 dioxane, 1-8 h, quant.; (c) 4-MeO-2-Me-phenylisocyanate, DIPEA, DCM or DMF, rt 4-24 h, 50-80%; (d) Boc-piperazine, DIPEA, NMP 110 °C 72 h, 49%; (e) 4M HCl in methanol, 4 h, quant.; (f) Boc-piperazine, DIPEA, 1,4 dioxane, 80 °C 4 h, 93.8%; (g) Sulfur, NH<sub>4</sub>OH, NMP, 90 °C 4 h, 79%; (h) MeNHNH<sub>2</sub>, THF, reflux 4 h, 47%.

Finally, in a bid to further improve potency and solubility within the series, the 5-membered ring adjacent to the hinge binding aminopyrimidine was investigated. Keeping the most potent piperazine urea combinations identified so far, analogues of **31a** were synthesized as detailed in Scheme 4. Deletion of the nitrogen of the thiazole ring to give the fused thiophene **35** gave a potent analogue, but thermodynamic solubility was negligible, and the hERG signal had further increased as LogD increased. Swapping the Sulfur of **31a** for an NMe group in purine analogue **38** (Scheme 4), gave a sub 10nM PI4KIII $\beta$  inhibitor, with HuMLR potency in line with that of **22**. Thermodynamic solubility was much improved with this hinge binding heterocycle, and no hERG or CYP3A4 inhibition observed.

**Table 5:** Profiling of hinge binder analogues of **31a**

| Cpd  | <b>35</b>  | <b>38</b>  | <b>42</b>   | <b>44</b>  |
|--|--|--|---|--|
|  |  |  |  |  |
| PI4KIII $\beta$ IC <sub>50</sub> (nM) <sup>a</sup> | 7  | 8  | 7   | 11   |
| Hu MLR IC <sub>50</sub> (nM) <sup>a</sup>          | 13   | 53   | 47  | 37   |
| Solubility-Kinetic ( $\mu$ M) <sup>b</sup>         | 82   | >350   | >350  | >350   |
| Solubility-TD ( $\mu$ M) <sup>c</sup>              | 0  | 150  | 52  | 110  |
| LogD (pH7.4)                                       | 2.39   | 1.35   | 1.96  | 1.47   |
| hERG IC <sub>50</sub> ( $\mu$ M)                   | 8 <sup>d</sup>   | >30  | 8   | >30  |
| CYP3A4 IC <sub>50</sub> ( $\mu$ M)                 | >20 <sup>d</sup>   | >20  | >20   | >20  |

<sup>a</sup>IC<sub>50</sub> values are reported as means of values from at least 2 determinations. <sup>b</sup>Kinetic solubility measured from DMSO stock at pH<sub>7.4</sub>.

<sup>c</sup>Thermodynamic solubility (TD) measured from solid stock at pH<sub>7.4</sub>. <sup>d</sup>Figures should be treated with caution due to low solubility.

The isothiazole **43** was also sub-10 nM against PI4KIII $\beta$ , although a drop off in the HuMLR was again noted. Thermodynamic solubility was modest, but as with **35**, a significant increase in the hERG signal was noted, although no CYP3A4 inhibition was present. Finally, the pyrazole

analogue **44** (UCB9608) was synthesized, and gave a good balance of potency and solubility, with no hERG or CYP flags as shown in Table 5. Compounds **31c**, **38** and **44** were chosen to be further evaluated *in vivo*. Prior to establishing mouse PK parameters, MLM and HLM stability was assessed. The addition of the chiral methyl piperazine to **22** (giving **31c**) had increased LogD, and metabolic stability was modestly impacted. The modifications made to the hinge binding region of **38** and **44** lowered LogD, and both MLM and HLM stability improved relative to **31c**. The efflux ratio (ER: Caco-2) for **22** and **38** indicated that these compounds were substrates for efflux transporters, whilst **31c** and **44** had a lower ER indicative of a reduced risk. Mouse PK was performed for the three compounds and data is shown in Table 6.

**Table 6:** Comparison of ADMET properties of **22** and analogues with improved solubility

| Compound  | <b>22</b>      | <b>31c</b> | <b>38</b>   | <b>44</b>   |
|---|----------------|------------|-------------|-------------|
| Hu MLR IC <sub>50</sub> (nM) <sup>a</sup>                       | 53             | 31         | 53          | 37          |
| Solubility-TD (μM) <sup>b</sup>                                 | 0              | 30         | 150         | 110         |
| LogD (pH7.4)  | 1.85           | 2.32       | 1.35        | 1.47        |
| MLM CL <sub>int</sub> (μl.min <sup>-1</sup> .mg <sup>-1</sup> ) | 15             | 35         | 10          | 6           |
| HLM CL <sub>int</sub> (μl.min <sup>-1</sup> .mg <sup>-1</sup> ) | 21             | 14         | 9           | 4           |
| Caco-2 ER <sup>c</sup>  | 5              | 1          | 5           | 2.6         |
| Fu (Mouse Blood)  | 0.061          | 0.020      | 0.200       | 0.090       |
| CL/F mL/min/kg (SD) <sup>d</sup>                                | 80 (±5)        | 42 (±12)   | 46 (±3)     | 5.3 (±0.7)  |
| AUC <sub>inf</sub> Free h.nM (SD) <sup>d</sup>                  | 332 (±18)      | 205 (±56)  | 1746 (±112) | 6941 (±887) |
| C <sub>max</sub> Free nM (SD) <sup>d</sup>                      | 154 (±24)      | 194 (±27)  | 1087 (±186) | 2113 (±259) |
| CL (mL/min/kg) <sup>e</sup>                                     | - <sup>f</sup> | 29 (±4.4)  | 19 (±4.0)   | 5 (±0.4)    |
| AUC Free h.nM (SD) <sup>e</sup>                                 | - <sup>f</sup> | 30 (±5)    | 447 (±86)   | 684 (±51)   |
| t <sub>1/2</sub> h <sup>e</sup>                                 | - <sup>f</sup> | 0.9 (±0.2) | 0.8 (±0.18) | 1.4 (±0.12) |
| V <sub>ss</sub> L/kg (SD) <sup>e</sup>                          | - <sup>f</sup> | 1.0 (±0.2) | 0.8 (±0.1)  | 0.6 (±0.04) |
| Oral F% <sup>g</sup>  | - <sup>f</sup> | 68         | 39          | ~100        |

<sup>a</sup>IC<sub>50</sub> values are reported as means of values from at least 2 determinations. <sup>c</sup>Calculated from Papp (A-B)/(B-A) in Caco-2 assay. <sup>d</sup>Oral PK established in male Balb/C mice, n=3 dosed at 10mpk in vehicle (0.1 % (w/v) Tween 80, 0.1 % (w/v) Silicone antifoam in 1 % (w/v) methylcellulose (400 cps) in water) as homogeneous suspensions of crystalline **31c**, **38** or **44**. <sup>e</sup>i.v PK established in Male Balb/C mice, n=3 dosed

1  
2  
3 at 1mpk in vehicle (30% DMA for **31c** and **38** or 15% NMP for **44**). <sup>f</sup>Too insoluble to formulate for i.v evaluation. <sup>g</sup>Bioavailability extrapolated  
4 from i.v/po experiments.  
5  
6

7 All three more soluble compounds showed low volume of distribution, and moderate to short  
8 half-lives. The higher LogD **31c**, had a higher CL<sub>b</sub> compared to other analogues, and so free drug  
9 levels following PO administration were no better than those seen with **22**, despite being well  
10 absorbed. Compound **38** although having a slightly lower CL<sub>b</sub> than **31c**, had a comparable half-  
11 life, impacted by its low volume of distribution. The bioavailability was also lower, which was  
12 unexpected due to the improved solubility and reduced clearance, and may have been due to  
13 reduced intestinal absorption, driven by active transport, in line with Caco-2 data. Compound **44**  
14 had very low CL<sub>b</sub>, commensurate with its low CL<sub>int</sub> in MLM, leading to a half-life of 1.4h, with  
15 high bioavailability, and low inter-individual variability. With its vastly improved oral PK profile  
16 in comparison to **22**, the pyrazolopyrimidine **44** appeared to be an excellent *in vivo* tool  
17 compound. AMES MPF<sup>66</sup> screening of **44** showed no flags and metabolic profiling in isolated  
18 human microsomes<sup>67</sup> again showed no evidence of urea hydrolysis or aniline derived  
19 metabolites. The embedded 2-methyl-4-methoxy aniline was also assessed in AMES MPF, and  
20 appeared free of risk<sup>68</sup>.  
21  
22  
23  
24  
25  
26  
27  
28  
29  
30  
31  
32  
33  
34  
35  
36  
37  
38  
39  
40  
41  
42  
43  
44  
45  
46  
47  
48  
49  
50  
51  
52  
53  
54  
55  
56  
57  
58  
59  
60



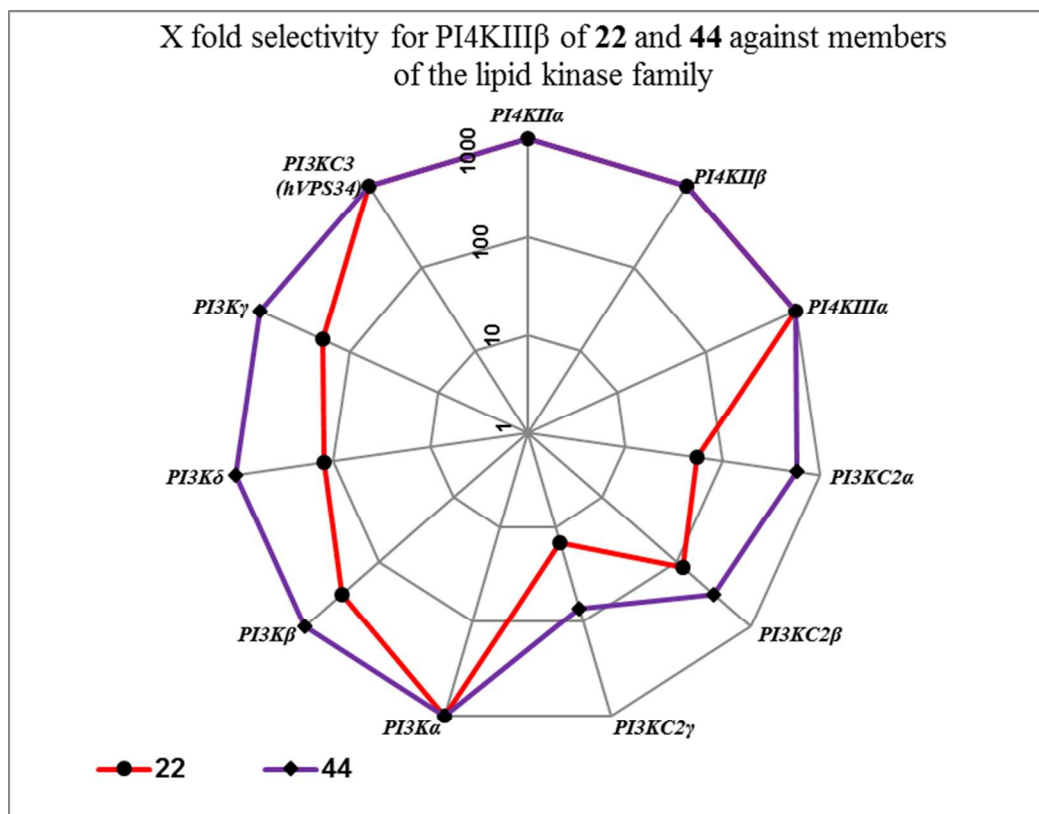


**Figure 6.** Radial plot showing the X-fold selectivity of **22** and **44** for PI4KIIIβ over 11 other lipid kinase family members

Kinome wide screening<sup>50</sup> of **44** was undertaken, and of the 250 kinases tested at 10 μM, only the PI4KIIIβ and PI3KC2 α, β and γ lipid kinases were inhibited. The selectivity profile of **44** for PI4KIIIβ over the 11 available lipid kinases confirmed that **44** had a much improved selectivity profile<sup>69</sup> in comparison to **22** (Figure 6). Throughout the discovery of **44**, UCB and Proteros<sup>70</sup> worked together to deliver a crystal structure of a piperazine urea inhibitor bound to PI4KIIIβ that would confirm a binding mode and rationalize the observed SAR. Initial efforts to solve the structure of any protein/ligand complex were hindered by the poor behavior of PI4KIIIβ toward crystallization. Several disordered regions were identified within the protein and it was envisaged that through reengineering of these flexible loops (a process also utilized to deliver recently published PI4KIIIβ/ligand complex structures<sup>32,42</sup>), constructs more amenable to crystallography could be obtained. It therefore proved possible to obtain the first crystals of a

1  
2  
3 urea (**44**) bound to human PI4KIII $\beta$ . These crystals consisted of 2 monomers of PI4KIII $\beta$  in the  
4 asymmetric unit, with one monomer (Chain A) being well defined, whilst the second monomer  
5 (Chain B) was highly disordered<sup>71</sup>. Clear density corresponding to the structure of **44** was visible  
6 in the kinase domain of the ordered monomer (Chain A), and was used for all subsequent  
7 analysis of the binding mode. As expected, the amino pyrimidine of **44** makes a bi-dentate  
8 interaction with the Val613 backbone, consistent with other published structures of amino  
9 heterocyclic inhibitors bound to PI4KIII $\beta$ <sup>42,44</sup>. Whereas the aryl and amide side chains of  
10 inhibitors such as **12**, reach along the ATP binding pocket toward Lys564 in one direction, and  
11 Asn615 in the other, **44** appears to orient the appended piperazine urea away from the pocket  
12 toward solvent (Figure 7). There is no contact with Lys564, Asn615 or Tyr385, residues believed  
13 to be critical for PI4KIII $\beta$  activity<sup>42</sup>, although it could be postulated that earlier urea analogues  
14 bearing an aryl or 3-pyridyl group on the hinge binding core could reach toward Lys564  
15 explaining the difference in potency between **14** and **22** (Table 1).  
16  
17  
18  
19  
20  
21  
22  
23  
24  
25  
26  
27  
28  
29  
30  
31  
32  
33  
34  
35  
36  
37  
38  
39  
40  
41  
42  
43  
44  
45  
46  
47  
48  
49  
50  
51  
52  
53  
54  
55  
56  
57  
58  
59  
60

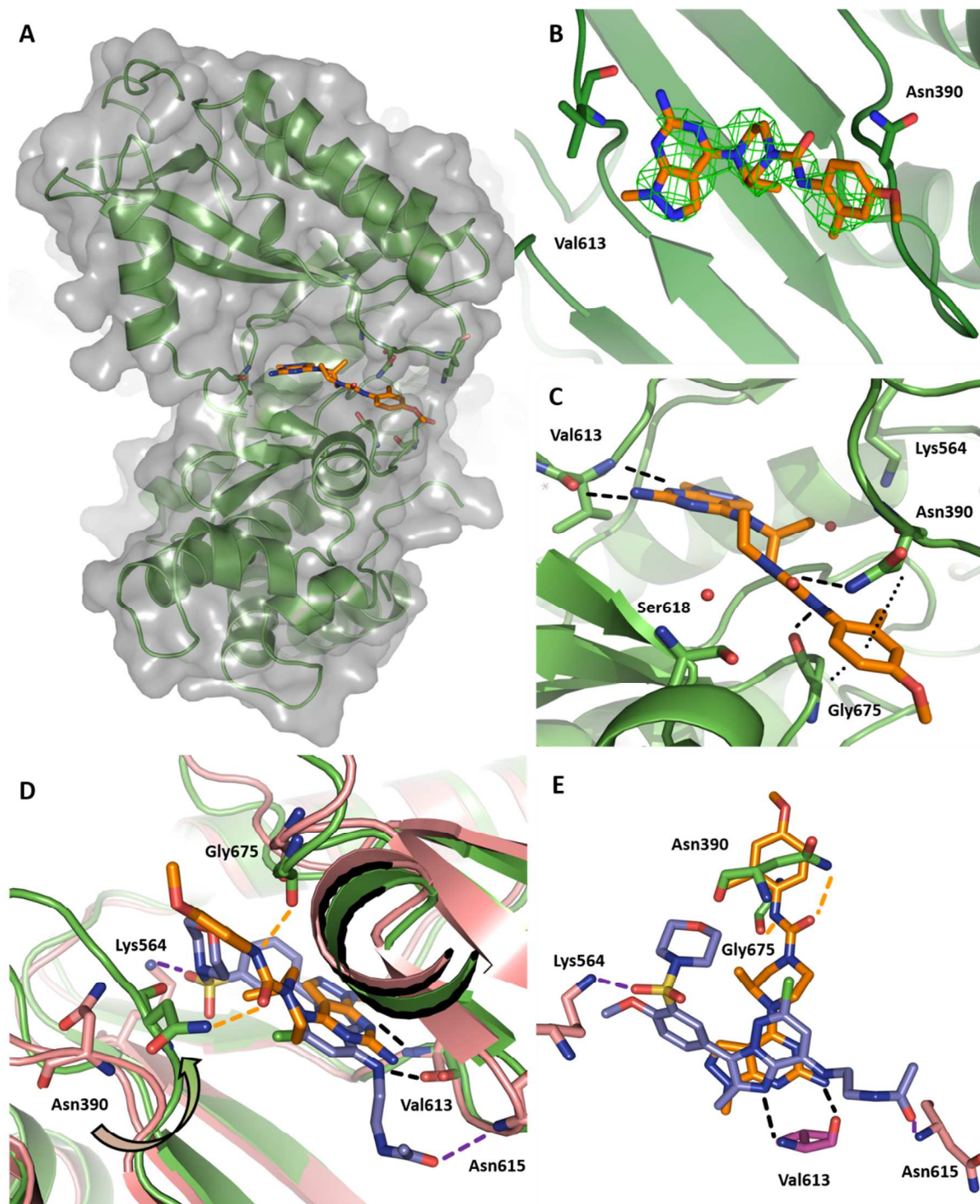


**Figure 7.** (A) Co-crystal of **44** (Orange) and PI4KIII $\beta$  (green) with surface superimposed in grey (PDB ID 6GL3). (B) The unbiased electron density ( $f_o-f_c$ , contoured at  $3\sigma$ ) of **44**. (C) Detailed view of the key protein/ligand interactions made by **44** (orange) with PI4KIII $\beta$  (green). H-bonds shown as dashed lines, C-H/ $\pi$  interactions as dotted lines. (D) Overlay of **44** (orange) and **12** (Purple) from published structure (5FBL). H-bond interactions shown as dashed lines (black for shared, orange for **44** specific and purple for **12** specific). Curved arrow denotes loop movement seen in structure of **44**. (E) Detailed overlay of **12** and **44** showing key residues involved in H-bonding, and the different direction of

1  
2  
3 growth from the hinge binding heterocyclic core of each ligand. Images generated using PyMol (The PyMOL Molecular Graphics System,  
4 Schrödinger, LLC).  
5

6  
7 As can be seen in Figure 7, the urea NH and carbonyl of **44** form H-bonds with the main chain  
8 Gly675 carbonyl and the side chain NH<sub>2</sub> of Asn390 respectively. A water molecule is also  
9 visible within hydrogen bonding range of the side chain OH of Ser618 and the urea carbonyl.  
10  
11 The Asn390 residue is part of a loop of protein that has shifted to enclose the electron rich  
12 aromatic ring of the urea in **44**, with the side chain methylene of Asn390 and the main chain  
13 methylene of Gly675 available to make putative C-H/ $\pi$  interactions from above and below.  
14  
15 These interactions made by the aryl urea of **44** and the loop-shifted protein could help rationalize  
16 the previously observed SAR. The conformation of the piperazine, the geometry of the urea  
17 carbonyl and NH, as well as the electronics of the aromatic ring all needed to be optimal to give  
18 the most potent compounds. For example, the change from a planar nitrogen to an *SP*<sup>3</sup> carbon in  
19 amide **23** meant that it could not deliver the -CONHAr group on the same vector as observed  
20 with **44**, resulting in a drastic loss of activity. The piperazine amides (Table 2) would also be  
21 unable to replicate the binding mode of **44**, and suffer similar drops in activity. The modest  
22 potency observed with **24d** was the exception, however it was not possible to confirm a binding  
23 mode for this compound. As discussed previously electron rich aniline urea's such as **22**  
24 appeared more potent against PI4KIII $\beta$ , whilst electron poor urea's such as **25b** or **25e** were  
25 significantly less active. This could be rationalized by urea's bearing electron donating  
26 substituents showing an increased propensity to stabilize the loop movement observed in Figure  
27 7, through strengthening of the C-H/ $\pi$  interactions<sup>72</sup> with the Asn390 side chain and Gly675  
28 backbone methylene's. Certainly, the observation that the most potent compounds bear both a  
29 methoxy and a methyl group, suggest the effect is additive, and explains the jump in potency  
30 observed from **22** to **25i**, although from examining the structure of **44**, there also appears to be an  
31  
32  
33  
34  
35  
36  
37  
38  
39  
40  
41  
42  
43  
44  
45  
46  
47  
48  
49  
50  
51  
52  
53  
54  
55  
56  
57  
58  
59  
60

1  
2  
3 element of space filling with this ortho substituent, suggesting further exploration in this area is  
4 warranted. From the crystal structure of **44**, it was also noted that the chiral methyl appended to  
5 the piperazine linker sat axial, and pointed into a small hydrophobic pocket within the active site.  
6  
7  
8  
9  
10 There was obviously a clear difference between the (*S*) and (*R*) enantiomers, based on the data  
11 generated with compounds **31a** and **31b** and this proved to be the case for **44** as well<sup>73</sup>. From  
12  
13  
14 experience and from examination of analogous structures in the CSD<sup>74</sup> the axial conformation  
15 for the chiral methyl attached to piperazine is energetically favored over the equatorial (results  
16 not shown). Docking was difficult for these compounds because the correct geometry for the  
17 piperazine nitrogen is required, and the pocket is open on two sides. A protocol using ring  
18 conformations generated using Corina<sup>75</sup>, minimized using the OPLS3 forcefield<sup>76</sup> and docked  
19 with Glide<sup>77</sup> was able to reproduce the crystallographic binding modes. Docking of the distomer  
20  
21  
22  
23  
24  
25  
26  
27  
28 **31b** resulted in only a slightly worse docking score than **31a** but with the methyl in the equatorial  
29 conformation. We assume that the high eudysmic ratio between these two compounds derives  
30 from higher strain energy of this conformation, combined with the fact that the methyl in the  
31 distomer does not fit into the hydrophobic pocket shown in the X-ray structure of **44**. This  
32 apparent preference for an axial substituent fitting into this small hydrophobic pocket goes some  
33 way to explain the loss of activity with the more complex substituted piperazines in Table 4. It  
34 remains to be seen if the binding mode of **44**, has any relevance to the biological profile of these  
35 specific PI4KIII $\beta$  inhibitors, and further evaluation of the immunological profile of PI4KIII $\beta$   
36 inhibitors with different binding modes and selectivity profiles is ongoing, and will be reported  
37 in future publications. To complete the assessment of **44**, it was taken into the murine model of  
38 cardiac allograft rejection, at a dose of 5mpk (PO). With the improved oral bioavailability and  
39 reduced inter-individual variability in exposure of **44**, graft survival rates were significantly  
40  
41  
42  
43  
44  
45  
46  
47  
48  
49  
50  
51  
52  
53  
54  
55  
56  
57  
58  
59  
60

improved as illustrated in Figure 8. Indeed, survival rates were unaffected after withdrawal of drug treatment at d14, with 90% of grafts being retained at day 50 (>36 days drug free) compared with a 50% survival rate for **22**. With **44** confirmed as a potent immunosuppressive agent, capable of prolonging heterotopic allograft retention *in vivo* it positions itself as an ideal tool compound to establish if PI4KIII $\beta$  inhibition can play a critical role in the development of future clinical immunosuppressive regimens.

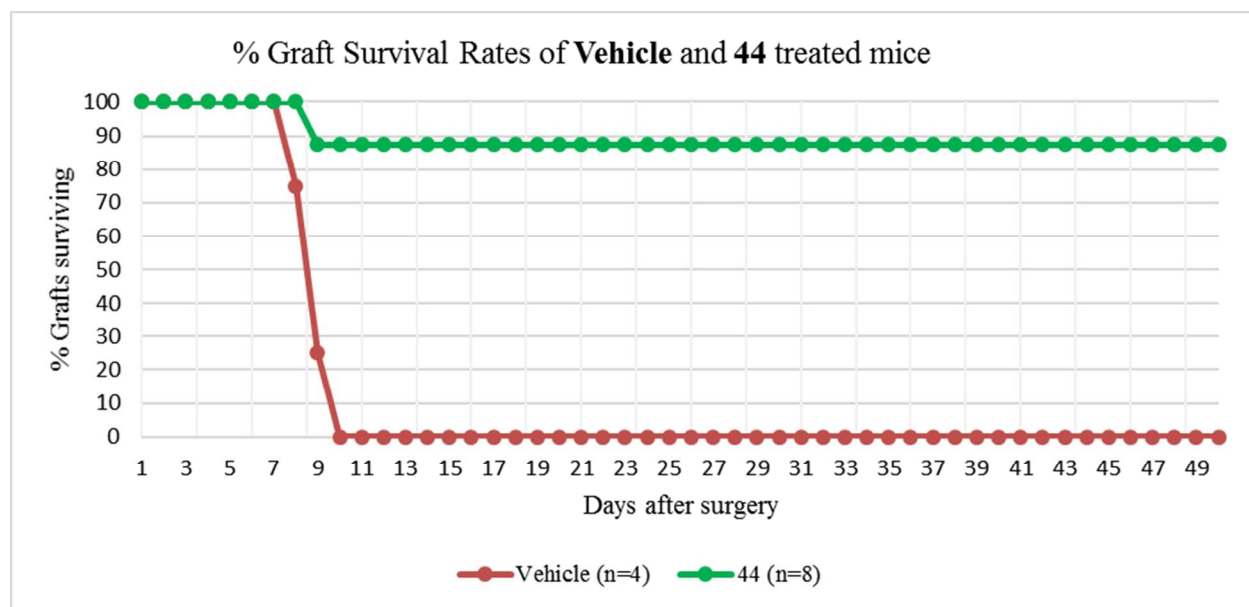


**Figure 8.** Comparison of survival rates for engrafted mice treated with vehicle (0.1 % (w/v) Tween 80, 0.1 % (w/v) Silicone antifoam in 1 % (w/v) methylcellulose (400 cps) in water), or **44** (5mpk in vehicle as a homogenous suspension). Animals were dosed via oral gavage once a day for 14 days, or until a transplanted graft had ceased beating, indicative of rejection. Graft survival is defined as a strongly beating heart (as confirmed by visual inspection and palpitation).

Further studies with **44** (UCB9608) and subsequent analogues are being explored, and will be discussed in future publications.

## CONCLUSION

Within this article, we have described the discovery **44** (UCB9608), an 11 nM PI4KIII $\beta$  inhibitor that inhibits the HuMLR response with an IC<sub>50</sub> of 37 nM. Its potency and excellent ADME properties make it an ideal compound for future use as an *in vitro* and *in vivo* probe to elucidate

1  
2  
3 the emerging role of PI4KIII $\beta$  inhibition in immune processes. Starting from a potent yet  
4 insoluble and poorly exposed chemotype we could address both hERG and CYP3A4 inhibition  
5 liabilities by the removal of a 3-pyridyl ring. Compound **22** was identified and its selectivity  
6 profile against the wider kinome and the close lipid kinase family established. Compound **22** was  
7 progressed to murine models of T-cell mediated antibody response, showing a dose dependent  
8 inhibition of IFN $\gamma$  release in a short-term mouse anti-CD3 model and significant inhibition of the  
9 oxazolone induced IgG1 response. At a dose of 100 mg/kg (PO), **22** facilitated the survival of a  
10 heterotopic murine cardiac allograft from a C57BL/6 donor mouse to a Balb/C H-2 recipient.  
11 Optimization and SAR exploration led to compound **44** (UCB9608), which could achieve high  
12 and consistently reproducible exposures in Balb/C mice. The structure of **44** bound to PI4KIII $\beta$   
13 was solved by co-crystallization, confirming that although **44** binds to the hinge region in an  
14 analogous fashion to other published PI4KIII $\beta$  inhibitors (such as **12**), it relies on a different H-  
15 bond network and unique CH/ $\pi$  interaction with a shifted protein loop to deliver low nM activity.  
16 Kinase cross screening confirmed **44** to be suitably selective for PI4KIII $\beta$  over other kinases,  
17 although the impact of low level activity against the PI3KC2 family was yet to be determined.  
18 Finally compound **44** could prevent the rejection of a heterotopic murine cardiac allograft at a  
19 dose of 5mpk. It is therefore our conclusion that **44** is an excellent example of a novel series of  
20 PI4KIII $\beta$  inhibitors that rely on a unique set of interactions within the binding site to drive  
21 potency. The excellent ADME properties of **44** make it an ideal molecule to develop the  
22 understanding of the role of this novel class of PI4KIII $\beta$  inhibitors on immune cell activation.  
23 Compound **44** (UCB9608) also offers an excellent platform to further develop the series as part  
24 of a potential CNI sparing treatment for the prevention of premature graft loss in solid organ  
25 transplantation and details of these efforts will be discussed in future publications.  
26  
27  
28  
29  
30  
31  
32  
33  
34  
35  
36  
37  
38  
39  
40  
41  
42  
43  
44  
45  
46  
47  
48  
49  
50  
51  
52  
53  
54  
55  
56  
57  
58  
59  
60

## Experimental Section

Reagents and solvents were purchased from commercial sources and used without purification. All final products were >95% pure as determined by HPLC-MS on an Agilent 1100 fitted with a Waters XBridge 20 x 2.1 mm, 2.5  $\mu\text{m}$  column. Mobile phase was (A) 10 mM ammonium formate in water + 0.1% ammonia and (B) acetonitrile +5% mobile phase A + 0.1% ammonia. A 5-minute gradient run (method 1: 5% B to 95% B in 3 minutes; hold until 4.00 minutes; at 4.01 minutes B concentration is 5%; hold until 5 minutes) or a 3-minute run (method 2: 5% B to 95% B in 1.5 minutes; hold until 2.5 minutes; at 2.51 minutes B concentration is 5%; hold until 3 minutes) were utilized.  $^1\text{H}$  NMR spectra were recorded at 300, 400 or 600 MHz and  $^{13}\text{C}$  NMR at 151 MHz on a Bruker spectrometer. Chemical shifts (ppm) were determined relative to internal solvent ( $^1\text{H}$ ,  $\delta$  2.50 ppm;  $\text{DMSO-}d_6$ ). Accurate Mass was determined by analysis of the samples on a calibrated Waters UPLC Xevo QToF. All animal experiments were conducted in accordance with the UK Home Office Animals (Scientific Procedures) Act 1986, with local ethical approval (in line with recently published guidelines) or with the approval of the Institutional Animal Care and Research Advisory Committee of the KU Leuven, Belgium.

**Synthesis of 13, 22, 25a-k, 31a-d, 35, 38, 42 and 44. General method 1** (Isocyanate-piperazine coupling reaction): To a solution of appropriate amine (0.74 mmol) in DMF (2 mL) or DCM (2 mL) was added  $\text{Et}_3\text{N}$  (2.20 mmol) or DIPEA (2.20 mmol) and the appropriate isocyanate (0.74 mmol). The reaction mixture was stirred at room temperature for 4 h. Upon completion, the reaction mixture was concentrated and the resulting material was purified by column chromatography (silica gel: 100-200 mesh,  $\text{MeOH:DCM}$  1:9) to afford the desired urea in yields between 20 and 95%. **General method 2** (CDI coupling): To a stirred solution of the appropriate amine (0.48 mmol) in DMF (1 mL) were added DIPEA (0.44 mmol) and CDI (0.48 mmol). The



1  
2  
3 reaction mixture was stirred at room temperature for 30 minutes. To this mixture was added a  
4 solution of **19b** (0.40 mmol) and DIPEA (0.48 mmol) in DMF (1 mL). The reaction mixture was  
5  
6 stirred at room temperature for a further 12 h. The reaction mixture was then diluted with EtOAc,  
7  
8 and the organic layer was washed with water and brine. The organic layer was dried over  
9  
10 anhydrous Na<sub>2</sub>SO<sub>4</sub>, concentrated *in vacuo* and the residue purified by column chromatography  
11  
12 (silica: 100-200 mesh, MeOH:DCM 5-7%) to afford the desired urea in yields between 20 and  
13  
14 95%. **General method 3** (Phenyl chloroformate coupling): To a solution of the appropriate  
15  
16 amine (1.05 mmol) in THF (5 mL) at 0°C was added pyridine (0.11 mL, 1.32 mmol), followed by  
17  
18 phenyl chloroformate (0.14 mL, 1.11 mmol). The reaction was stirred at 0°C for 2 h, then diluted  
19  
20 with EtOAc and washed successively with 2M HCl solution. The organic layer was concentrated  
21  
22 *in vacuo* and the resultant crude phenyl carbamate and **19b** (1 equivalent) were taken up in  
23  
24 DMSO (2 mL) and DIPEA (3 equivalents) added. The mixture was warmed to 60°C and stirred  
25  
26 for 3 h. After this time the reaction was cooled, and diluted with EtOAc and washed with water.  
27  
28 The organic layer was dried over Na<sub>2</sub>SO<sub>4</sub> and concentrated *in vacuo*, and the residue purified by  
29  
30 column chromatography (silica: 100-200 mesh, MeOH:DCM 5-7%) to afford the desired urea in  
31  
32 yields between 50 and 90%.  
33  
34  
35  
36  
37  
38  
39  
40

#### 41 **4-[5-Amino-2-(3-pyridyl)thiazolo[5,4-*d*]pyrimidin-7-yl]-*N*-(*p*-tolyl)piperazine-1-**

42 **carboxamide (13)** was synthesized from **21b** and 4-methylphenyl isocyanate according to  
43  
44 general method 1. <sup>1</sup>H NMR (600 MHz, DMSO-*d*<sub>6</sub>) δ 9.13 (dd, J = 0.9, 2.4 Hz, 1H), 8.67 (dd, J =  
45  
46 1.6, 4.8 Hz, 1H), 8.49 (s, 1H), 8.29 (ddd, J = 1.6, 2.4, 8.0 Hz, 1H), 7.56 (ddd, J = 0.9, 4.9, 8.1 Hz,  
47  
48 1H), 7.40 – 7.34 (m, 2H), 7.09 – 7.03 (m, 2H), 6.57 (s, 2H), 4.31 (s, 4H), 3.66 – 3.60 (m, 4H),  
49  
50 2.24 (s, 3H). <sup>13</sup>C NMR (151 MHz, DMSO) δ 168.58, 160.62, 155.51, 155.09, 151.19, 150.35,  
51  
52  
53  
54  
55  
56  
57  
58  
59  
60

1  
2  
3 147.34, 138.29, 133.98, 131.06, 129.62, 129.21, 125.35, 124.68, 120.25, 45.50, 44.14, 20.83.

4  
5 HRMS: calcd for C<sub>22</sub>H<sub>22</sub>N<sub>8</sub>OS [M+H]<sup>+</sup>, 447.1716; found, 447.1697.

6  
7  
8  
9 **4-(5-Aminothiazolo[5,4-*d*]pyrimidin-7-yl)-*N*-(4-methoxyphenyl)piperazine-1-carboxamide**

10 (22) was synthesized from **19b** and 4-methoxyphenyl isocyanate according to general method 1.

11  
12  
13 <sup>1</sup>H NMR (600 MHz, DMSO-*d*<sub>6</sub>) δ 8.71 (s, 1H), 8.43 (s, 1H), 7.39 – 7.33 (m, 2H), 6.89 – 6.81 (m,  
14 2H), 6.39 (s, 2H), 4.24 (s, 4H), 3.71 (s, 3H), 3.59 – 3.54 (m, 4H). <sup>13</sup>C NMR (151 MHz, DMSO) δ  
15 167.59, 160.62, 155.74, 155.38, 155.01, 143.30, 133.78, 124.68, 122.15, 114.01, 55.58, 45.38,  
16 44.07. HRMS: calcd for C<sub>17</sub>H<sub>19</sub>N<sub>7</sub>O<sub>2</sub>S [M+H]<sup>+</sup>, 386.1399; found, 386.1395.  
17  
18  
19  
20  
21  
22

23 **4-(5-Aminothiazolo[5,4-*d*]pyrimidin-7-yl)-*N*-phenyl-piperazine-1-carboxamide (25a)** was

24 synthesized from **19b** and phenyl isocyanate according to general Method 1. <sup>1</sup>H NMR (600  
25 MHz, DMSO-*d*<sub>6</sub>) δ 8.72 (s, 1H), 8.58 (s, 1H), 7.50 – 7.45 (m, 2H), 7.28 – 7.22 (m, 2H), 6.97 –  
26 6.94 (m, 1H), 6.40 (s, 2H), 4.25 (s, 4H), 3.62 – 3.57 (m, 4H). <sup>13</sup>C NMR (151 MHz, DMSO) δ  
27 167.59, 160.62, 155.47, 155.38, 143.31, 140.87, 128.79, 124.68, 122.28, 120.15, 45.64, 44.16.  
28  
29  
30  
31  
32  
33  
34  
35 HRMS: calcd for C<sub>16</sub>H<sub>17</sub>N<sub>7</sub>OS [M+H]<sup>+</sup>, 356.1294; found, 356.1303.  
36  
37

38 **4-(5-Aminothiazolo[5,4-*d*]pyrimidin-7-yl)-*N*-(3-pyridyl)piperazine-1-carboxamide (25b)**

39 was synthesized from **19b** and 3-pyridylisocyanate according to general method 1. <sup>1</sup>H NMR (600  
40 MHz, DMSO-*d*<sub>6</sub>) δ 8.79 (s, 1H), 8.72 (s, 1H), 8.66 (d, *J* = 2.6 Hz, 1H), 8.17 (dd, *J* = 1.5, 4.7 Hz,  
41 1H), 7.90 (ddd, *J* = 1.6, 2.7, 8.4 Hz, 1H), 7.29 (dd, *J* = 4.6, 8.3 Hz, 1H), 6.41 (s, 2H), 4.26 (s,  
42 4H), 3.64 – 3.59 (m, 4H). <sup>13</sup>C NMR (151 MHz, DMSO) δ 167.61, 160.62, 155.39, 155.28,  
43 143.35, 143.29, 141.86, 137.57, 126.96, 124.68, 123.70, 45.38, 44.09. HRMS: calcd for  
44  
45  
46  
47  
48  
49  
50  
51  
52 C<sub>15</sub>H<sub>16</sub>N<sub>8</sub>OS [M+H]<sup>+</sup>, 357.1246; found, 357.1243.  
53  
54  
55  
56  
57  
58  
59  
60

**4-(5-Aminothiazolo[5,4-*d*]pyrimidin-7-yl)-*N*-(6-methoxy-3-pyridyl)piperazine-1-**

**carboxamide (25c)** was synthesized from **19b** and 6-methoxypyridin-3-amine according to general method 2. <sup>1</sup>H NMR (600 MHz, DMSO-*d*<sub>6</sub>) δ 8.71 (s, 1H), 8.58 (s, 1H), 8.20 (d, *J* = 2.7 Hz, 1H), 7.77 (dd, *J* = 2.7, 8.9 Hz, 1H), 6.76 (d, *J* = 8.8 Hz, 1H), 6.40 (s, 2H), 4.27 – 4.23 (m, 4H), 3.81 (s, 3H), 3.61 – 3.56 (m, 4H). <sup>13</sup>C NMR (151 MHz, DMSO) δ 167.60, 160.62, 159.56, 155.74, 155.38, 143.34, 138.86, 133.19, 131.54, 124.67, 110.08, 53.51, 45.40, 44.01. HRMS: calcd for C<sub>16</sub>H<sub>18</sub>N<sub>8</sub>O<sub>2</sub>S [M+H]<sup>+</sup>, 387.1352; found, 387.1322.

**4-(5-Aminothiazolo[5,4-*d*]pyrimidin-7-yl)-*N*-[(4-methoxyphenyl)methyl]piperazine-1-**

**carboxamide (25d)** was synthesized from **19b** and 4-methoxybenzyl isocyanate according to general method 1. <sup>1</sup>H NMR (600 MHz, DMSO-*d*<sub>6</sub>) δ 8.70 (s, 1H), 7.27 – 7.14 (m, 2H), 7.09 (t, *J* = 5.8 Hz, 1H), 6.92 – 6.82 (m, 2H), 6.37 (s, 2H), 4.30 – 4.04 (m, 6H), 3.72 (s, 3H), 3.52 – 3.42 (m, 4H). <sup>13</sup>C NMR (151 MHz, DMSO) δ 167.56, 160.60, 158.46, 157.87, 155.37, 143.27, 133.30, 132.06, 128.84, 113.98, 55.50, 45.50, 43.88, 43.40. HRMS: calcd for C<sub>18</sub>H<sub>21</sub>N<sub>7</sub>O<sub>2</sub>S [M+H]<sup>+</sup>, 400.1556; found, 400.1537.

**4-(5-Aminothiazolo[5,4-*d*]pyrimidin-7-yl)-*N*-[4-(trifluoromethoxy)phenyl]piperazine-1-**

**carboxamide (25e)** was synthesized from **19b** and 4-trifluoromethoxyphenyl isocyanate according to general method 1. <sup>1</sup>H NMR (600 MHz, DMSO-*d*<sub>6</sub>) δ 8.79 (s, 1H), 8.71 (s, 1H), 7.62 – 7.56 (m, 2H), 7.29 – 7.23 (m, 2H), 6.40 (s, 2H), 4.25 (s, 4H), 3.62 – 3.57 (m, 4H). <sup>13</sup>C NMR (151 MHz, DMSO) δ 167.60, 160.62, 155.38, 155.29, 143.34, 143.07, 140.24, 124.67, 121.70, 121.11, 99.99, 45.38, 44.12. HRMS: calcd for C<sub>17</sub>H<sub>16</sub>F<sub>3</sub>N<sub>7</sub>O<sub>2</sub>S [M+H]<sup>+</sup>, 440.1117; found, 440.1108.

1  
2  
3 **4-(5-Aminothiazolo[5,4-*d*]pyrimidin-7-yl)-*N*-(*o*-tolyl)piperazine-1-carboxamide (25f)** was  
4 synthesized from **19b** and 2-methylphenyl isocyanate according general method 1. <sup>1</sup>H NMR (600  
5 MHz, DMSO-*d*<sub>6</sub>) δ 8.71 (s, 1H), 8.11 (s, 1H), 7.24 - 7.17 (m, 2H), 7.14 (td, *J* = 1.6, 7.7 Hz, 1H),  
6 7.06 (td, *J* = 1.4, 7.4 Hz, 1H), 6.40 (s, 2H), 4.25 (s, 4H), 3.61 – 3.55 (m, 4H), 2.19 (s, 3H). <sup>13</sup>C  
7 NMR (151 MHz, DMSO) δ 167.59, 160.63, 156.05, 155.42, 143.31, 138.28, 133.60, 130.53,  
8 126.48, 126.25, 125.13, 124.69, 45.32, 44.24, 18.42. HRMS: calcd for C<sub>17</sub>H<sub>19</sub>N<sub>7</sub>OS [M+H]<sup>+</sup>,  
9 370.1450; found, 370.1442.

10  
11  
12 **4-(5-Aminothiazolo[5,4-*d*]pyrimidin-7-yl)-*N*-(*m*-tolyl)piperazine-1-carboxamide (25g)** was  
13 synthesized from **19b** and 3-methylphenyl isocyanate according general method 1. <sup>1</sup>H NMR (600  
14 MHz, DMSO-*d*<sub>6</sub>) δ 8.71 (s, 1H), 8.51 (s, 1H), 7.31 (s, 1H), 7.28 (d, *J* = 8.1 Hz, 1H), 7.13 (t, *J* =  
15 7.8 Hz, 1H), 6.77 (d 7.5 Hz, 1H), 6.40 (s, 2H), 4.24 (s, 4H), 3.61 – 3.55 (m, 4H), 2.26 (s, 3H).  
16 <sup>13</sup>C NMR (151 MHz, DMSO) δ 167.59, 160.62, 155.46, 155.38, 143.31, 140.77, 137.81, 128.64,  
17 124.67, 123.01, 120.74, 117.30, 45.47, 44.15, 21.67. HRMS: calcd for C<sub>17</sub>H<sub>19</sub>N<sub>7</sub>OS [M+H]<sup>+</sup>,  
18 370.1450; found, 370.1446.

19  
20  
21 **4-(5-Aminothiazolo[5,4-*d*]pyrimidin-7-yl)-*N*-(*p*-tolyl)piperazine-1-carboxamide (25h)** was  
22 synthesized from **19b** and 4-methylphenyl isocyanate according to general method 1. <sup>1</sup>H NMR  
23 (600 MHz, DMSO-*d*<sub>6</sub>) δ 8.71 (s, 1H), 8.48 (s, 1H), 7.38 – 7.32 (m, 2H), 7.08 – 7.03 (m, 2H),  
24 6.40 (s, 2H), 4.24 (s, 4H), 3.60 – 3.55 (m, 4H), 2.24 (s, 3H). <sup>13</sup>C NMR (151 MHz, DMSO) δ  
25 167.59, 160.62, 155.55, 155.38, 143.30, 138.25, 131.09, 129.21, 124.68, 120.36, 45.42, 44.10,  
26 20.82. HRMS: calcd for C<sub>17</sub>H<sub>19</sub>N<sub>7</sub>OS [M+H]<sup>+</sup>, 370.1450; found, 370.1436.

27  
28  
29 **4-(5-Aminothiazolo[5,4-*d*]pyrimidin-7-yl)-*N*-(4-methoxy-2-methylphenyl)piperazine-1-**  
30 **carboxamide (25i)** was synthesized from **19b** and 4-methoxy-2-methylphenyl isocyanate  
31  
32  
33  
34  
35  
36  
37  
38  
39  
40  
41  
42  
43  
44  
45  
46  
47  
48  
49  
50  
51  
52  
53  
54  
55  
56  
57  
58  
59  
60

1  
2  
3 according to general method 1.  $^1\text{H}$  NMR (600 MHz, DMSO- $d_6$ )  $\delta$  8.71 (s, 1H), 8.01 (s, 1H), 7.06  
4 (d,  $J = 8.6$  Hz, 1H), 6.78 (d,  $J = 2.9$  Hz, 1H), 6.71 (dd,  $J = 3.0, 8.6$  Hz, 1H), 6.40 (s, 2H), 4.24 (s,  
5 4H), 3.73 (s, 3H), 3.58 – 3.53 (m, 4H), 2.15 (s, 3H).  $^{13}\text{C}$  NMR (151 MHz, DMSO)  $\delta$  167.59,  
6 160.63, 157.08, 156.46, 155.41, 143.30, 135.87, 131.05, 128.42, 124.67, 115.62, 111.45, 55.55,  
7 45.06, 44.20, 18.61. HRMS: calcd for  $\text{C}_{18}\text{H}_{21}\text{N}_7\text{O}_2\text{S}$   $[\text{M}+\text{H}]^+$ , 400.1561; found, 400.1549.  
8  
9

10  
11  
12 **4-(5-Aminothiazolo[5,4-*d*]pyrimidin-7-yl)-*N*-(6-methoxy-4-methyl-3-pyridyl)piperazine-1-**  
13 **carboxamide (25j)** was synthesized from **19b** and 6-methoxy-4-methyl-pyridin-3-amine  
14 according to general method 3.  $^1\text{H}$  NMR (600 MHz, DMSO- $d_6$ )  $\delta$  8.71 (s, 1H), 8.19 (s, 1H),  
15 7.89 (s, 1H), 6.70 (s, 1H), 6.40 (s, 2H), 4.25 (s, 4H), 3.81 (s, 3H), 3.60 – 3.55 (m, 4H), 2.15 (s,  
16 3H).  $^{13}\text{C}$  NMR (151 MHz, DMSO)  $\delta$  167.60, 161.74, 160.63, 156.46, 155.42, 147.87, 144.71,  
17 143.33, 129.67, 124.68, 110.93, 53.52, 45.35, 44.20, 18.00. HRMS: calcd for  $\text{C}_{17}\text{H}_{20}\text{N}_8\text{O}_2\text{S}$   
18  $[\text{M}+\text{H}]^+$ , 401.1508; found, 401.1505.  
19  
20  
21  
22  
23  
24  
25  
26  
27  
28  
29  
30

31  
32 **4-(5-Aminothiazolo[5,4-*d*]pyrimidin-7-yl)-*N*-(6-methoxy-2-methyl-3-pyridyl)piperazine-1-**  
33 **carboxamide (25k)** was synthesized from **19b** and 6-methoxy-2-methyl-pyridin-3-amine  
34 according to general method 3.  $^1\text{H}$  NMR (600 MHz, DMSO- $d_6$ )  $\delta$  8.71 (s, 1H), 8.16 (s, 1H),  
35 7.46 (d,  $J = 8.6$  Hz, 1H), 6.61 (d,  $J = 8.5$  Hz, 1H), 6.40 (s, 2H), 4.25 (s, 4H), 3.82 (s, 3H), 3.60 –  
36 3.55 (m, 4H), 2.29 (s, 3H).  $^{13}\text{C}$  NMR (151 MHz, DMSO)  $\delta$  167.60, 160.62, 160.55, 156.25,  
37 155.41, 151.90, 143.33, 138.72, 127.77, 124.68, 107.69, 53.48, 45.28, 44.15, 21.21. HRMS:  
38 calcd for  $\text{C}_{17}\text{H}_{20}\text{N}_8\text{O}_2\text{S}$   $[\text{M}+\text{H}]^+$ , 401.1508; found, 401.1506.  
39  
40  
41  
42  
43  
44  
45  
46  
47  
48

49 **(3*S*)-4-(5-Aminothiazolo[5,4-*d*]pyrimidin-7-yl)-*N*-(4-methoxy-2-methyl-phenyl)-3-methyl-**  
50 **piperazine-1-carboxamide (31a)** was synthesized from **30a** and 4-methoxy-2-methylphenyl  
51 isocyanate according to general method 1.  $^1\text{H}$  NMR (600 MHz, DMSO- $d_6$ )  $\delta$  8.71 (s, 1H), 7.98  
52  
53  
54  
55  
56  
57  
58  
59  
60

(s, 1H), 7.04 (d, J = 8.6 Hz, 1H), 6.78 (d, J = 2.9 Hz, 1H), 6.71 (dd, J = 3.0, 8.6 Hz, 1H), 6.37 (s, 2H), 5.60 (s, 1H), 5.15 (s, 1H), 4.15 – 4.11 (m, 1H), 4.01 – 3.96 (m, 1H), 3.73 (s, 3H), 3.38 (s, 1H), 3.26 (dd, J = 3.9, 13.4 Hz, 1H), 3.08 – 3.02 (m, 1H), 2.15 (s, 3H), 1.26 (d, J = 6.6 Hz, 3H). <sup>13</sup>C NMR (151 MHz, DMSO) δ 167.63, 160.64, 157.13, 156.57, 155.28, 143.14, 136.05, 131.09, 128.58, 124.59, 115.61, 111.47, 55.55, 47.91, 44.00, 40.53, 40.39, 18.55, 15.57. HRMS: calcd for C<sub>19</sub>H<sub>23</sub>N<sub>7</sub>O<sub>2</sub>S [M+H]<sup>+</sup>, 414.1712; found, 414.1708.

**(3R)-4-(5-Aminothiazolo[5,4-d]pyrimidin-7-yl)-N-(4-methoxy-2-methyl-phenyl)-3-methyl-piperazine-1-carboxamide (31b)** was synthesized from **30b** and 4-methoxy-2-methylphenyl isocyanate according to general method 1. <sup>1</sup>H NMR (600 MHz, DMSO-d<sub>6</sub>) δ 8.71 (s, 1H), 7.98 (s, 1H), 7.04 (d, J = 8.6 Hz, 1H), 6.78 (d, J = 2.9 Hz, 1H), 6.71 (dd, J = 3.0, 8.6 Hz, 1H), 6.37 (s, 2H), 5.60 (s, 1H), 5.15 (s, 1H), 4.15 – 4.11 (m, 1H), 4.01 – 3.96 (m, 1H), 3.73 (s, 3H), 3.38 (s, 1H), 3.26 (dd, J = 3.9, 13.4 Hz, 1H), 3.08 – 3.02 (m, 1H), 2.15 (s, 3H), 1.26 (d, J = 6.6 Hz, 3H). <sup>13</sup>C NMR (151 MHz, DMSO) δ 167.63, 160.64, 157.13, 156.57, 155.28, 143.14, 136.05, 131.09, 128.58, 124.59, 115.61, 111.47, 55.55, 47.91, 44.00, 40.53, 40.39, 18.55, 15.57. HRMS: calcd for C<sub>19</sub>H<sub>23</sub>N<sub>7</sub>O<sub>2</sub>S [M+H]<sup>+</sup>, 414.1712; found, 414.1708.

**(3S)-4-(5-aminothiazolo[5,4-d]pyrimidin-7-yl)-N-(4-methoxyphenyl)-3-methyl-piperazine-1-carboxamide (31c)** was synthesized from **30a** and 4-methoxyphenyl isocyanate according to general method 1. <sup>1</sup>H NMR (600 MHz, DMSO-d<sub>6</sub>) δ 8.71 (s, 1H), 8.38 (s, 1H), 7.38 – 7.33 (m, 2H), 6.87 – 6.82 (m, 2H), 6.37 (s, 2H), 5.58 (s, 1H), 5.15 (s, 1H), 4.15 – 4.09 (m, 1H), 4.02 – 3.96 (m, 1H), 3.71 (s, 3H), 3.45 – 3.34 (m, 1H), 3.25 (dd, J = 4.0, 13.4 Hz, 1H), 3.09 – 3.03 (m, 1H), 1.23 (d, J = 6.6 Hz, 3H). <sup>13</sup>C NMR (151 MHz, DMSO) δ 167.62, 160.63, 156.08, 155.23, 155.03, 143.15, 133.77, 124.59, 122.27, 113.99, 55.59, 47.78, 44.12, 40.38, 40.24, 15.80. HRMS: calcd for C<sub>18</sub>H<sub>21</sub>N<sub>7</sub>O<sub>2</sub>S [M+H]<sup>+</sup>, 400.1556; found, 400.1541.

**(3*S*)-4-(5-aminothiazolo[5,4-*d*]pyrimidin-7-yl)-*N*-(6-methoxy-2-methyl-3-pyridyl)-3-methyl-piperazine-1-carboxamide (31d)** was synthesized from **30a** and 6-methoxy-2-methyl-pyridin-3-amine according to general method 3. <sup>1</sup>H NMR (600 MHz, DMSO-*d*<sub>6</sub>) δ 8.71 (s, 1H), 8.12 (s, 1H), 7.44 (d, *J* = 8.5 Hz, 1H), 6.61 (d, *J* = 8.5 Hz, 1H), 6.37 (s, 2H), 5.60 (s, 1H), 5.16 (s, 1H), 4.17 – 4.09 (m, 1H), 4.01 – 3.96 (m, 1H), 3.82 (s, 3H), 3.43 – 3.38 (m, 1H), 3.29 (dd, *J* = 4.0, 13.5 Hz, 1H), 3.11 – 3.04 (m, 1H), 2.29 (s, 3H), 1.26 (d, *J* = 6.6 Hz, 3H). <sup>13</sup>C NMR (151 MHz, DMSO) δ 167.64, 160.63, 160.60, 156.36, 155.27, 152.07, 143.18, 138.86, 127.80, 124.61, 107.72, 53.49, 47.89, 43.98, 40.53, 40.38, 21.13, 15.71. HRMS: calcd for C<sub>18</sub>H<sub>22</sub>N<sub>8</sub>O<sub>2</sub>S [M+H]<sup>+</sup>, 415.1665; found, 415.1645.

**(3*S*)-4-(2-aminothieno[2,3-*d*]pyrimidin-4-yl)-*N*-(4-methoxy-2-methyl-phenyl)-3-methyl-piperazine-1-carboxamide (35)** was synthesized from **34** and 4-methoxy-2-methylphenyl isocyanate according to general method 1. <sup>1</sup>H NMR (600 MHz, DMSO-*d*<sub>6</sub>) δ 7.97 (s, 1H), 7.33 (d, *J* = 6.2 Hz, 1H), 7.06 – 7.00 (m, 2H), 6.78 (d, *J* = 2.9 Hz, 1H), 6.71 (dd, *J* = 3.1, 8.6 Hz, 1H), 6.19 (s, 2H), 4.80 – 4.74 (m, 1H), 4.35 – 4.29 (m, 1H), 4.09 – 4.00 (m, 1H), 3.96 – 3.88 (m, 1H), 3.73 (s, 3H), 3.47 – 3.40 (m, 1H), 3.33 – 3.27 (m, 1H), 3.17 – 3.09 (m, 1H), 2.14 (s, 3H), 1.28 (d, *J* = 6.7 Hz, 3H). <sup>13</sup>C NMR (151 MHz, DMSO) δ 172.32, 160.22, 158.84, 157.09, 156.61, 136.00, 131.12, 128.51, 122.00, 115.61, 115.28, 111.46, 108.80, 55.56, 49.82, 47.76, 43.62, 40.68, 18.55, 15.75. HRMS: calcd for C<sub>20</sub>H<sub>24</sub>N<sub>6</sub>O<sub>2</sub>S [M+H]<sup>+</sup>, 413.1760; found, 413.1756.

**(3*S*)-4-(2-amino-9-methyl-purin-6-yl)-*N*-(4-methoxy-2-methyl-phenyl)-3-methyl-piperazine-1-carboxamide (38)** was synthesized from **37** and 4-methoxy-2-methylphenyl isocyanate according to general method 1. <sup>1</sup>H NMR (600 MHz, DMSO-*d*<sub>6</sub>) δ 7.97 (s, 1H), 7.73 (s, 1H), 7.03 (d, *J* = 8.6 Hz, 1H), 6.78 (d, *J* = 2.9 Hz, 1H), 6.71 (dd, *J* = 3.0, 8.6 Hz, 1H), 5.91 (s, 2H), 5.55 (s, 1H), 5.04 (s, 1H), 4.17 – 4.12 (m, 1H), 4.02 – 3.98 (m, 1H), 3.73 (s, 3H), 3.56 (s, 3H), 3.31 –

1  
2  
3 3.22 (m, 1H), 3.19 (dd, J = 3.8, 13.4 Hz, 1H), 3.00 – 2.92 (m, 1H), 2.15 (s, 3H), 1.22 (d, J = 6.7  
4 Hz, 3H). <sup>13</sup>C NMR (151 MHz, DMSO) δ 160.07, 157.11, 156.58, 153.95, 153.93, 137.83,  
5  
6 136.07, 131.15, 128.60, 115.61, 113.75, 111.46, 55.55, 48.03, 44.06, 40.53, 40.39, 29.51, 18.56,  
7  
8 15.40. HRMS: calcd for C<sub>20</sub>H<sub>26</sub>N<sub>8</sub>O<sub>2</sub> [M+H]<sup>+</sup>, 411.2257; found, 411.2258.  
9  
10  
11

12  
13 **2-Amino-4-[4-(4-methoxy-2-methylphenylcarbamoyl)-2-(S)-methylpiperazin-1-yl]-**  
14

15 **isothiazolo[5,4-d]pyrimidine (42)** was synthesized from **41** and 4-methoxy-2-methylphenyl  
16 isocyanate according to general method 1. <sup>1</sup>H NMR (600 MHz, DMSO-d<sub>6</sub>) δ 8.91 (s, 1H), 8.00  
17 (s, 1H), 7.04 (d, J = 8.6 Hz, 1H), 6.78 (d, J = 2.9 Hz, 1H), 6.74 (s, 2H), 6.73 - 6.69 (m, 1H), 4.90  
18 – 4.81 (m, 1H), 4.49 – 4.40 (m, 1H), 4.09 – 4.02 (m, 1H), 3.98 – 3.93 (m, 1H), 3.73 (s, 3H), 3.60  
19 – 3.51 (m, 1H), 3.41 – 3.31 (m, 1H), 3.25 – 3.18 (m, 1H), 2.14 (s, 3H), 1.31 (d, J = 6.6 Hz, 3H).  
20  
21 <sup>13</sup>C NMR (151 MHz, DMSO) δ 184.06, 161.38, 158.76, 157.12, 156.59, 154.25, 136.00, 131.07,  
22  
23 128.50, 115.62, 111.48, 108.12, 55.56, 47.49, 43.48, 40.53, 40.39, 18.55, 16.25. HRMS: calcd  
24  
25 for C<sub>19</sub>H<sub>23</sub>N<sub>7</sub>O<sub>2</sub>S [M+H]<sup>+</sup>, 414.1712; found, 414.1706.  
26  
27  
28  
29  
30  
31  
32  
33

34  
35 **(3S)-4-(6-amino-1-methyl-pyrazolo[3,4-d]pyrimidin-4-yl)-N-(4-methoxy-2-methyl-phenyl)-**  
36

37 **3-methyl-piperazine-1-carboxamide (44)** was synthesized from **43** and 4-methoxy-2-  
38 methylphenyl isocyanate according to general method 1. <sup>1</sup>H NMR (600 MHz, DMSO-d<sub>6</sub>) δ 8.00  
39 (s, 1H), 7.93 (s, 1H), 7.04 (d, J = 8.6 Hz, 1H), 6.78 (d, J = 3.0 Hz, 1H), 6.71 (dd, J = 3.0, 8.6 Hz,  
40 1H), 6.20 (s, 2H), 4.97 – 4.58 (m, 1H), 4.58 – 4.20 (m, 1H), 4.13 – 4.06 (m, 1H), 4.01 – 3.95 (m,  
41 1H), 3.73 (s, 3H), 3.71 (s, 3H), 3.44 – 3.32 (m, 1H), 3.31 – 3.25 (m, 1H), 3.14 – 3.07 (m, 1H),  
42 2.15 (s, 3H), 1.24 (d, J = 6.7 Hz, 3H). <sup>13</sup>C NMR (101 MHz, DMSO, 100°C) δ 161.99, 157.67,  
43  
44 157.61, 157.34, 156.82, 135.63, 133.06, 131.46, 128.20, 115.97, 111.77, 95.53, 55.81, 48.98,  
45  
46 47.81, 43.88, 41.19, 33.40, 18.33, 15.96. HRMS: calcd for C<sub>20</sub>H<sub>26</sub>N<sub>8</sub>O<sub>2</sub> [M+H]<sup>+</sup>, 411.2257;  
47  
48 found, 411.2254.  
49  
50  
51  
52  
53  
54  
55  
56  
57  
58  
59  
60



## Biological screening assays

**The Mixed Lymphocyte Reaction (MLR) Test:** Human peripheral blood mononuclear cells (PBMCs) were isolated from buffy coats, obtained from healthy blood donors by Ficoll (Lymphoprep, Axis-Shield PoC AS, Oslo, Norway) density-gradient centrifugation. The cells at the Ficoll-plasma interface were washed three times and used as “Responder” cells. RPMI 1788 (ATCC, N° CCL-20 156) cells were treated with mitomycin C (Kyowa, Nycomed, Brussels, Belgium) and used as “Stimulator” cells. Responder cells ( $0.12 \times 10^6$ ), Stimulator cells ( $0.045 \times 10^6$ ) and compounds (in different concentrations) were cocultured for 6 days in RPMI 1640 medium (BioWhittaker, Lonza, Belgium) supplemented with 10% fetal calf serum, 100 U/ml Geneticin (Gibco, LifeTechnologies, UK). Cells were cultured in triplicate in flat-bottomed 96-well microtiter tissue culture plates (TTP, Switzerland). After 5 days, cells were pulsed with 1  $\mu\text{Ci}$  of methyl- $^3\text{H}$  thymidine (MP Biomedicals, USA), harvested after 18 h, on glass filter paper and counted. Proliferation values were expressed as counts per minute (cpm), and converted to % inhibition with respect to a blank MLR test (identical but without added compound). The  $\text{IC}_{50}$  was determined from a graph with at least four points, each derived from the mean of 2 experiments. The  $\text{IC}_{50}$  value represents the lowest concentration of test compound (expressed in  $\mu\text{M}$ ) that resulted in a 50% inhibition of the MLR.

**PI4KIII $\beta$  Enzyme Inhibition Assay:** Compounds were screened in 1% DMSO (final) as 3-fold serial dilutions from a starting concentration of 20  $\mu\text{M}$ . PI4KIII $\beta$ , PI Lipid Kinase Substrate (both Invitrogen, Paisley UK), ATP (Promega, Southampton, UK) and the 5X compounds were prepared in 20 mM Tris pH 7.5, 0.5 mM EGTA, 2 mM DTT, 5 mM  $\text{MgCl}_2$ , 0.4% Triton (all Sigma, Dorset, UK). The final 25  $\mu\text{L}$  kinase reaction consisted of: 4 nM PI4KIII $\beta$ , 100  $\mu\text{M}$  PI Lipid Kinase Substrate (both Invitrogen), and compound. The final ATP concentration in the

1  
2  
3 assay was 10  $\mu$ M. Briefly, compound was added to PI4KIII $\beta$  followed by addition of ATP/PI  
4 Lipid Kinase Substrate mixture. The reaction mixture was incubated for 60 minutes at room  
5  
6 temperature. The ADP-Glo™ Reagent was added and the plate was incubated for 40 minutes at  
7  
8 room temperature, followed by addition of ADP-Glo™ Detect Reagent (both Promega,  
9  
10 Southampton, UK). The plate was incubated for a further 120 minutes and luminescence read on  
11  
12 a plate reader. The IC<sub>50</sub> values were generated with a 4PL fit using XLfit software.  
13  
14

15  
16 ***In vitro* DMPK methods and hERG screening:** For methods pertaining to measuring  
17  
18 microsomal clearances (human and mouse), blood binding (mouse), passive permeability (Caco-  
19  
20 2) and cytochrome P450 inhibition (3A4 and other isoforms) see methods as describe by  
21  
22 Cyprotex (: <http://www.cyprotex.com/admeprk>, (accessed May 23<sup>rd</sup>, 2018). hERG Screening was  
23  
24 carried out by B'SYS: [http://www.bsys.ch/services/ion-channel-screening/patch-clamping/herg-](http://www.bsys.ch/services/ion-channel-screening/patch-clamping/herg-cho.html)  
25  
26 [cho.html](http://www.bsys.ch/services/ion-channel-screening/patch-clamping/herg-cho.html), (accessed May 23<sup>rd</sup>, 2018).  
27  
28

29  
30 **Evaluation in murine heart allograft model:** Inbred C57BL/6 H-2b and Balb/C female mice,  
31  
32 8-10 weeks old, between 20 and 25 g were used as donor and recipient respectively. Heterotopic  
33  
34 heart and transplantation was performed by implanting the donor heart on the neck of the  
35  
36 recipients using conventional microsurgery techniques as described previously<sup>78</sup>. Grafts were  
37  
38 implanted in the recipient neck, and graft beating was checked daily by inspection and  
39  
40 palpitation. Cessation of beating indicated graft rejection, which was confirmed by histological  
41  
42 examination. Housing and all experimental animal procedures were approved by the Institutional  
43  
44 Animal Care and Research Advisory Committee of the KU Leuven, Belgium.  
45  
46  
47  
48  
49

### 50 **Structural determination of 44 bound to PI4KIII $\beta$**

51  
52 **Protein Production for crystallography:** For structure analysis, a crystallization system was  
53  
54 developed for the kinase domain of PI4KIII $\beta$ , in which amino acids 429-531 of PI4KIII $\beta$  were  
55  
56  
57  
58  
59  
60

1  
2  
3 replaced by a short linker sequence. In summary<sup>79</sup> protein carrying an N-terminal TEV-cleavable  
4 HIS-GST-fusion was expressed in baculovirus-infected insect cells and purified by a three-step  
5 procedure comprising affinity and size exclusion chromatography steps. Protein for  
6 crystallization was concentrated to 15-20 mg/mL in crystallization buffer (20 mM  
7 HEPES/NaOH, pH=7.0, 150 mM NaCl, 10% glycerol, 5 mM DTT) and stored in small aliquots  
8 at 193 K.  
9

10  
11 **Crystallization and Structure analysis:** Crystals of PI4KIII $\beta$  in complex with **44** were grown  
12 by mixing protein solution (12.5 mg/ml + 0.5 mM TCEP + 5 mM MgCl<sub>2</sub> + 2 mM ligand **44**) with  
13 reservoir solution (0.2 M sodium citrate, 22% (w/v) PEG3350, 10 mM Manganese(II)chloride)  
14 in a 1:1 ratio at 293 K. Before flash freezing in liquid nitrogen, crystals were cryo protected by  
15 immersing them in reservoir solution supplemented with 20% (v/v) PEG200. Diffraction data of  
16 the complex were collected at the Swiss Light Source (SLS, Villigen, Switzerland). The  
17 structure was solved to a final resolution of 2.77 Å. The phase information necessary to  
18 determine and analyse the structure was obtained by molecular replacement using a previously  
19 solved structure of PI4KIII $\beta$  as a search model<sup>80</sup>. Subsequent model building and refinement was  
20 performed according to standard protocols with CCP4<sup>81</sup> and COOT<sup>82</sup>. Ligand parameterisation  
21 and generation was carried out with CORINA<sup>83</sup>. The water model was built with the “find  
22 waters2” algorithm of COOT, followed by refinement with REFMAC5<sup>84</sup> and checking all waters  
23 with the validation tool of COOT. The crystals contain two monomers of human PI4KIII $\beta$   
24 protein (Chain A and Chain B) in the asymmetric unit with only one of the two protein  
25 monomers having ligand **44** bound (Chain A). Chain A is well-defined by electron density, with  
26 an average B-factor after TLS analysis of 56.86. In Chain B, lacking a bound ligand, the  
27 electron density is much weaker and a large portion of the N-lobe is poorly defined (average B-  
28  
29  
30  
31  
32  
33  
34  
35  
36  
37  
38  
39  
40  
41  
42  
43  
44  
45  
46  
47  
48  
49  
50  
51  
52  
53  
54  
55  
56  
57  
58  
59  
60

factor of 95.77<sup>71</sup>), hence the higher than normal R factors observed ( $R [\%] / R_{\text{free}} [\%] = 27.6 / 33.3$ ), given the resolution of the structure (2.77 Å). Full data collection, processing, and refinement statistics for the structure of **44** bound to human PI4KIII $\beta$  are given in the supporting information.

## ASSOCIATED CONTENT

### Supporting Information:

For full experimental details and characterization of intermediates **16**, **17**, **18**, **19a**, **19b**, **20**, **21a**, **21b**, **29a**, **29b**, **30a**, **30b**, **33**, **34**, **37**, **40**, **41**, **43** and compounds **11**, **23**, **24a-f** and **28a-g**, a full list of molecular formula strings, further details on the structural determination of PI4KIII $\beta$  with **44** (including refinement statistics), kinase profiling of **2**, **13**, **22** and **44**, details of physicochemical assays used, reactive metabolite screening method and results for **22** and **44** and the *in vivo* methods for anti-CD3 and OXA models see the **Supporting Information**.

### Accession Codes

The atomic co-ordinates and structure factors for compound **44** (UCB9608) are deposited in the RCSB Protein Data Bank, [www.pdb.org](http://www.pdb.org) (accession code 6GL3), and authors will release the atomic coordinates and experimental data upon article publication.

## AUTHOR INFORMATION

### Corresponding Author

\*James Reuberson: phone, +44-1753-534655; e-mail, [james.reuberson@ucb.com](mailto:james.reuberson@ucb.com)

The author declares no competing financial interest.

Current contact details for Shenggiao Li: [lishq26@mail.sysu.edu.cn](mailto:lishq26@mail.sysu.edu.cn).

1  
2  
3 Current contact details for Bart Vanderhoydonck are: Center for Drug Design and Discovery  
4 Bioincubator 2, Gaston Geenslaan 2, 3001 Leuven, Belgium.

### 7 **Acknowledgement**

8  
9  
10 Special thanks to Rodger Allen, Johnny Zhu and Jeremy Davis for their support and guidance.  
11 Recognition to Anant Ghawalkar and the SAI team for their synthetic contributions, to Justin  
12 Staniforth, Richard Taylor and Harry Mackenzie and the PASG team for analytical support,  
13 Mike King for CADD input and discussions and Doug Byrne and Sukhjit Sohal for help with  
14 standard synthesis. Thanks also to Alex Ferecsko, Sophie Kervyn, Lloyd King, Franck Atienza  
15 and Helga Gerets for their help in formulation, safety profiling and establishing met ID. In  
16 memory of PLR.  
17  
18  
19  
20  
21  
22  
23  
24  
25

### 26 **ABBREVIATIONS USED**

27  
28  
29  
30  
31 ADME, absorption, distribution, metabolism and excretion; AUC, area under the curve; Boc.  
32 Tert-butoxy carbamate; CDI, carbonyl diimidazole; CNI, calcineurin inhibitor; Cps, cycles per  
33 second, CSA, Cyclosporin A; CYP, Cytochrome P; DBU, 1,8-Diazabicyclo[5.4.0]undec-7-ene;  
34 DCM, dichloromethane; DDI, drug-drug interaction; DIPEA, diisopropylethylamine; DMF,  
35 dimethylformamide; DMSO, dimethylsulfoxide; EDCI, 1-Ethyl-3-(3-  
36 dimethylaminopropyl)carbodiimide; ELISA, enzyme-linked immunosorbent assay; Et<sub>3</sub>N,  
37 triethylamine; EtOAc, ethylacetate; FU, fraction unbound; HATU, 1-  
38 [Bis(dimethylamino)methylene]-1H-1,2,3-triazolo[4,5-b]pyridinium 3-oxid  
39 hexafluorophosphate; HBA, hydrogen bond acceptor; HBD, hydrogen bond donor; HLM, human  
40  
41  
42  
43  
44  
45  
46  
47  
48  
49  
50  
51  
52  
53  
54  
55  
56  
57  
58  
59  
60

1  
2  
3 liver microsomes; HOBT, hydroxybenzotriazole; HuMLR, human Mixed lymphocyte reaction;  
4  
5  
6 IFN, interferon; MeOH, methanol; MLM, mouse liver microsomes; MMF, Mycophenolate  
7  
8  
9 mofetil; MPF, multi-plate format; mpk, mg's per kg; NADPH, Nicotinamide adenine  
10  
11  
12 dinucleotide phosphate; NBS, N-Bromosuccinamide; NMP, N-methylpyrrolidinone; PI3KC1,  
13  
14 phosphoinositol-3-kinase class 1; PI3KC2, phosphoinositol-3-kinase class 2; PI4KIII $\beta$ ,  
15  
16 phosphoinositol-4-kinase class 3 beta; PK, pharmacokinetic; PO, *per os*; PyBOP, (Benzotriazol-  
17  
18 1-yloxy)tripyrrolidinophosphonium hexafluorophosphate; SAR, structure activity relationship.  
19  
20  
21  
22  
23

## 24 **References**

- 25  
26  
27 (1) Dangoor, J. Y.; Hakim, D. N.; Singh, R. P.; Hakim, N. S. Transplantation: A Brief History.  
28  
29 *Experimental and Clinical Transplantation : Official Journal of the Middle East Society for*  
30  
31 *Organ Transplantation* **2015**, *13*, 1-5.  
32  
33  
34 (2) Agarwal, A.; Ally, W.; Brayman, K. The Future Direction and Unmet Needs of Transplant  
35  
36 Immunosuppression. *Expert Review of Clinical Pharmacology* **2016**, *9*, 873-876.  
37  
38  
39 (3) Billingham, R. E.; Krohn, P. L.; Medawar, P. B. Effect of Cortisone on Survival of Skin  
40  
41 Homografts in Rabbits. *British Medical Journal* **1951**, *1*, 1157-1163.  
42  
43  
44 (4) Borel, J. F.; Kis, Z. L. The Discovery and Development of Cyclosporine (Sandimmune).  
45  
46 *Transplantation Proceedings* **1991**, *23*, 1867-1874.  
47  
48  
49 (5) Goto, T.; Kino, T.; Hatanaka, H.; Nishiyama, M.; Okuhara, M.; Kohsaka, M.; Aoki, H.;  
50  
51 Imanaka, H. Discovery of FK-506, a Novel Immunosuppressant Isolated from *Streptomyces*  
52  
53 *Tsukubaensis*. *Transplantation Proceedings* **1987**, *19*, 4-8.  
54  
55  
56  
57  
58  
59  
60

- 1  
2  
3 (6) Sollinger, H. W. Mycophenolates in Transplantation. *Clinical Transplantation* **2004**, *18*, 485-  
4  
5 492.  
6  
7  
8 (7) Salvadori, M.; Bertoni, E. Is it Time to Give Up with Calcineurin Inhibitors in Kidney  
9  
10 Transplantation? *World Journal of Transplantation* **2013**, *3*, 7-25.  
11  
12 (8) Klintmalm, G. B.; Vincenti, F.; Kirk, A. Steroid-Responsive Acute Rejection Should Not Be  
13  
14 the End Point for Immunosuppressive Trials. *American Journal of Transplantation: Official*  
15  
16 *Journal of the American Society of Transplantation and the American Society of Transplant*  
17  
18 *Surgeons* **2016**, *16*, 3077-3078.  
19  
20  
21 (9) Flechner, S. M.; Kobashigawa, J.; Klintmalm, G. Calcineurin Inhibitor-Sparing Regimens in  
22  
23 Solid Organ Transplantation: Focus on Improving Renal Function and Nephrotoxicity. *Clinical*  
24  
25 *Transplantation* **2008**, *22*, 1-15.  
26  
27  
28 (10) Jang, M. Y.; Lin, Y.; De Jonghe, S.; Gao, L. J.; Vanderhoydonck, B.; Froeyen, M.;  
29  
30 Rozenski, J.; Herman, J.; Louat, T.; Van Belle, K.; Waer, M.; Herdewijn, P. Discovery of 7-N-  
31  
32 piperazinylthiazolo[5,4-d]pyrimidine Analogues as a Novel Class of Immunosuppressive Agents  
33  
34 with in Vivo Biological Activity. *Journal of Medicinal Chemistry* **2011**, *54*, 655-668.  
35  
36  
37 (11) Ghobrial, II; Morris, A. G.; Booth, L. J. Clinical Significance of in Vitro Donor-Specific  
38  
39 Hyporesponsiveness in Renal Allograft Recipients as Demonstrated by the MLR. *Transplant*  
40  
41 *International: Official Journal of the European Society for Organ Transplantation* **1994**, *7*, 420-  
42  
43 427.  
44  
45  
46 (12) Ferraris, J.; Tambutti, M.; Prigoshin, N. Improved Long-Term Graft Function in Kidney  
47  
48 Transplant Recipients with Donor Antigen-Specific Hyporeactivity. *Pediatric Transplantation*  
49  
50 **2007**, *11*, 139-144.  
51  
52  
53  
54  
55  
56  
57  
58  
59  
60

- 1  
2  
3 (13) Thomas, F. T.; Lee, H. M.; Lower, R. R.; Thomas, J. M. Immunological Monitoring as a  
4 Guide to the Management of Transplant Recipients. *The Surgical Clinics of North America* **1979**,  
5  
6 *59*, 253-281.  
7  
8  
9  
10 (14) Cerep (now Eurofins): <https://www.eurofinsdiscoveryservices.com/> accessed May 23<sup>rd</sup>,  
11  
12 2018.  
13  
14 (15) DiscoverX: <https://www.discoverx.com/home/> accessed May 23<sup>rd</sup>, 2018.  
15  
16  
17 (16) Full details of the kinase profiling of **2** can be found within the accompanying supporting  
18  
19 information.  
20  
21 (17) Heath, C. M.; Stahl, P. D.; Barbieri, M. A. Lipid Kinases Play Crucial and Multiple Roles in  
22  
23 Membrane Trafficking and Signaling. *Histology and Histopathology* **2003**, *18*, 989-998.  
24  
25  
26 (18) Heilmeyer, L. M., Jr.; Vereb, G., Jr.; Vereb, G.; Kakuk, A.; Szivak, I. Mammalian  
27  
28 Phosphatidylinositol 4-Kinases. *IUBMB Life* **2003**, *55*, 59-65.  
29  
30  
31 (19) Balla, T. Phosphoinositides: Tiny Lipids With Giant Impact on Cell Regulation.  
32  
33 *Physiological Reviews* **2013**, *93*, 1019-1137.  
34  
35  
36 (20) Delang, L.; Paeshuyse, J.; Neyts, J. The Role of Phosphatidylinositol 4-Kinases and  
37  
38 Phosphatidylinositol 4-Phosphate During Viral Replication. *Biochemical Pharmacology* **2012**,  
39  
40 *84*, 1400-1408.  
41  
42  
43 (21) McNamara, C. W.; Lee, M. C.; Lim, C. S.; Lim, S. H.; Roland, J.; Nagle, A.; Simon, O.;  
44  
45 Yeung, B. K.; Chatterjee, A. K.; McCormack, S. L. Targeting Plasmodium PI(4)K to Eliminate  
46  
47 Malaria. *Nature* **2013**, *504*, 248-253.  
48  
49  
50 (22) Boura, E.; Nencka, R. Phosphatidylinositol 4-Kinases: Function, Structure, and Inhibition.  
51  
52 *Experimental Cell Research* **2015**, *337*, 136-145.  
53  
54  
55  
56  
57  
58  
59  
60



- 1  
2  
3 (23) Klima, M.; Toth, D. J.; Hexnerova, R.; Baumlova, A.; Chalupska, D.; Tykvart, J.;  
4  
5 Rezaczkova, L.; Sengupta, N.; Man, P.; Dubankova, A.; Humpolickova, J.; Nencka, R.; Veverka,  
6  
7 V.; Balla, T.; Boura, E. Structural Insights and in Vitro Reconstitution of Membrane Targeting  
8  
9 and Activation of Human PI4KB by the ACBD3 Protein. *Scientific Reports* **2016**, *6*, 23641.
- 10  
11 (24) Sridhar, S.; Patel, B.; Aphkhazava, D.; Macian, F.; Santambrogio, L.; Shields, D.; Cuervo,  
12  
13 A. M. The Lipid Kinase PI4KIIIbeta Preserves Lysosomal Identity. *The EMBO Journal* **2013**,  
14  
15 *32*, 324-339.
- 16  
17 (25) Toth, B.; Balla, A.; Ma, H.; Knight, Z. A.; Shokat, K. M.; Balla, T. Phosphatidylinositol 4-  
18  
19 Kinase IIIbeta Regulates the Transport of Ceramide Between the Endoplasmic Reticulum and  
20  
21 Golgi. *The Journal of Biological Chemistry* **2006**, *281*, 36369-36377.
- 22  
23 (26) Dornan, G. L.; McPhail, J. A.; Burke, J. E. Type III Phosphatidylinositol 4 Kinases:  
24  
25 Structure, Function, Regulation, Signalling and Involvement in Disease. *Biochemical Society*  
26  
27 *Transactions* **2016**, *44*, 260-266.
- 28  
29 (27) Klima, M.; Chalupska, D.; Rozycki, B.; Humpolickova, J.; Rezaczkova, L.; Silhan, J.;  
30  
31 Baumlova, A.; Dubankova, A.; Boura, E. Kobuviral Non-Structural 3A Proteins act as Molecular  
32  
33 Harnesses to Hijack the Host ACBD3 Protein. *Structure (London, England : 1993)* **2017**, *25*,  
34  
35 219-230.
- 36  
37 (28) McPhail, J. A.; Ottosen, E. H.; Jenkins, M. L.; Burke, J. E. The Molecular Basis of Aichi  
38  
39 Virus 3A Protein Activation of Phosphatidylinositol 4 Kinase IIIbeta, PI4KB, Through ACBD3.  
40  
41 *Structure (London, England : 1993)* **2017**, *25*, 121-131.
- 42  
43 (29) Dubankova, A.; Humpolickova, J.; Klima, M.; Boura, E. Negative Charge and Membrane-  
44  
45 Tethered Viral 3B Cooperate to Recruit Viral RNA Dependent RNA Polymerase 3D (pol).  
46  
47 *Scientific Reports* **2017**, *7*, 17309.
- 48  
49  
50  
51  
52  
53  
54  
55  
56  
57  
58  
59  
60

1  
2  
3 (30) Knight, Z. A.; Gonzalez, B.; Feldman, M. E.; Zunder, E. R.; Goldenberg, D. D.; Williams,  
4 O.; Loewith, R.; Stokoe, D.; Balla, A.; Toth, B.; Balla, T.; Weiss, W. A.; Williams, R. L.;  
5 Shokat, K. M. A Pharmacological Map of the PI3-K Family Defines a Role for p110alpha in  
6 Insulin Signaling. *Cell* **2006**, *125*, 733-747.  
7  
8  
9

10  
11 (31) Fowler, M. L.; McPhail, J. A.; Jenkins, M. L.; Masson, G. R.; Rutaganira, F. U.; Shokat, K.  
12 M.; Williams, R. L.; Burke, J. E. Using Hydrogen Deuterium Exchange Mass Spectrometry to  
13 Engineer Optimized Constructs for Crystallization of Protein Complexes: Case Study of  
14 PI4KIIIbeta with Rab11. *Protein Science : A Publication of the Protein Society* **2016**, *25*, 826-  
15 839.  
16  
17  
18  
19  
20  
21  
22

23 (32) Burke, J. E.; Inglis, A. J.; Perisic, O.; Masson, G. R.; McLaughlin, S. H.; Rutaganira, F.;  
24 Shokat, K. M.; Williams, R. L. Structures of PI4KIIIbeta Complexes Show Simultaneous  
25 Recruitment of Rab11 and its Effectors. *Science (New York, N.Y.)* **2014**, *344*, 1035-1038.  
26  
27  
28  
29

30 (33) Rutaganira, F. U.; Fowler, M. L.; McPhail, J. A.; Gelman, M. A.; Nguyen, K.; Xiong, A.;  
31 Dornan, G. L.; Tavshanjian, B.; Glenn, J. S.; Shokat, K. M.; Burke, J. E. Design and Structural  
32 Characterization of Potent and Selective Inhibitors of Phosphatidylinositol 4-Kinase IIIbeta.  
33 *Journal of Medicinal Chemistry* **2016**, *59*, 1830-1839.  
34  
35  
36  
37  
38

39 (34) Lamarche, M. J.; Borawski, J.; Bose, A.; Capacci-Daniel, C.; Colvin, R.; Dennehy, M.;  
40 Ding, J.; Dobler, M.; Drumm, J.; Gaither, L. A.; Gao, J.; Jiang, X.; Lin, K.; McKeever, U.;  
41 Puyang, X.; Raman, P.; Thohan, S.; Tommasi, R.; Wagner, K.; Xiong, X.; Zabawa, T.; Zhu, S.;  
42 Wiedmann, B. Anti-hepatitis C Virus Activity and Toxicity of Type III Phosphatidylinositol 4-  
43 Kinase Beta Inhibitors. *Antimicrobial Agents and Chemotherapy* **2012**, *56*, 5149-5156.  
44  
45  
46  
47  
48  
49

50 (35) Keaney, E. P.; Connolly, M.; Dobler, M.; Karki, R.; Honda, A.; Sukup, S.; Karur, S.; Britt,  
51 S.; Patnaik, A.; Raman, P.; Hamann, L. G.; Wiedmann, B.; LaMarche, M. J. 2-Alkyloxazoles as  
52  
53  
54  
55  
56  
57  
58  
59  
60

Potent and Selective PI4KIIIbeta Inhibitors Demonstrating Inhibition of HCV Replication. *Bioorganic & Medicinal Chemistry Letters* **2014**, *24*, 3714-3718.

(36) Decor, A.; Grand-Maitre, C.; Hucke, O.; O'Meara, J.; Kuhn, C.; Constantineau-Forget, L.; Brochu, C.; Malenfant, E.; Bertrand-Laperle, M.; Bordeleau, J.; Ghio, E.; Pesant, M.; Fazal, G.; Gorys, V.; Little, M.; Boucher, C.; Bordeleau, S.; Turcotte, P.; Guo, T.; Garneau, M.; Spickler, C.; Gauthier, A. Design, Synthesis and Biological Evaluation of Novel Aminothiazoles as Antiviral Compounds Acting Against Human Rhinovirus. *Bioorganic & Medicinal Chemistry Letters* **2013**, *23*, 3841-3847.

(37) Raubo, P.; Andrews, D. M.; McKelvie, J. C.; Robb, G. R.; Smith, J. M.; Swarbrick, M. E.; Waring, M. J. Discovery of Potent, Selective Small Molecule Inhibitors of Alpha-Subtype of type III Phosphatidylinositol 4-Kinase (PI4KIIIalpha). *Bioorganic & Medicinal Chemistry Letters* **2015**, *25*, 3189-3193.

(38) Waring, M. J.; Andrews, D. M.; Faulder, P. F.; Flemington, V.; McKelvie, J. C.; Maman, S.; Preston, M.; Raubo, P.; Robb, G. R.; Roberts, K.; Rowlinson, R.; Smith, J. M.; Swarbrick, M. E.; Treinies, I.; Winter, J. J.; Wood, R. J. Potent, Selective Small Molecule Inhibitors of Type III Phosphatidylinositol 4-Kinase Alpha but not Beta Inhibit the Phosphatidylinositol Signaling Cascade and Cancer Cell Proliferation. *Chemical Communications (Cambridge, England)* **2014**, *50*, 5388-5390.

(39) Arita, M.; Kojima, H.; Nagano, T.; Okabe, T.; Wakita, T.; Shimizu, H. Phosphatidylinositol 4-Kinase III Beta is a Target of Enviroxime-Like Compounds for Antipoliiovirus Activity. *Journal of Virology* **2011**, *85*, 2364-2372.

(40) Catalano, J. G.; Gaitonde, V.; Beesu, M.; Leivers, A. L.; Shotwell, J. B. Phenoxide Leaving Group SNAr Strategy for the Facile Preparation of 7-Amino-3-aryl Pyrazolo[1,5-a]pyrimidines

1  
2  
3 from a 3-Bromo-7-phenoxy-pyrazolo[1,5-a]pyrimidine Intermediate. *Tetrahedron Letters* **2015**,  
4  
5 *56*, 6077-6079.

6  
7  
8 (41) Leivers, A.L. Chemical Optimization of Novel Inhibitor Classes Selectively Targeting  
9  
10 PI4KIII $\beta$ : A Novel Host Lipid Kinase Crucial for Enterovirus Replication. Presented at the 249th  
11  
12 National Meeting of the American Chemical Society, Denver, Colorado, March 25th, 2015.

13  
14 (42) Mejdrova, I.; Chalupska, D.; Plackova, P.; Muller, C.; Sala, M.; Klima, M.; Baumlova, A.;  
15  
16 Hrebabecky, H.; Prochazkova, E.; Dejmek, M.; Strunin, D.; Weber, J.; Lee, G.; Matousova, M.;  
17  
18 Mertlikova-Kaiserova, H.; Ziebuhr, J.; Birkus, G.; Boura, E.; Nencka, R. Rational Design of  
19  
20 Novel Highly Potent and Selective Phosphatidylinositol 4-Kinase IIIbeta (PI4KB) Inhibitors as  
21  
22 Broad-Spectrum Antiviral Agents and Tools for Chemical Biology. *Journal of Medicinal*  
23  
24 *Chemistry* **2017**, *60*, 100-118.

25  
26  
27 (43) Humpolickova, J.; Mejdrova, I.; Matousova, M.; Nencka, R.; Boura, E. Fluorescent  
28  
29 Inhibitors as Tools to Characterize Enzymes: Case Study of the Lipid Kinase  
30  
31 Phosphatidylinositol 4-Kinase IIIbeta (PI4KB). *Journal of Medicinal Chemistry* **2017**, *60*, 119-  
32  
33 127.

34  
35  
36 (44) Mejdrova, I.; Chalupska, D.; Kogler, M.; Sala, M.; Plackova, P.; Baumlova, A.;  
37  
38 Hrebabecky, H.; Prochazkova, E.; Dejmek, M.; Guillon, R.; Strunin, D.; Weber, J.; Lee, G.;  
39  
40 Birkus, G.; Mertlikova-Kaiserova, H.; Boura, E.; Nencka, R. Highly Selective  
41  
42 Phosphatidylinositol 4-Kinase IIIbeta Inhibitors and Structural Insight into Their Mode of  
43  
44 Action. *Journal of Medicinal Chemistry* **2015**, *58*, 3767-3793.

45  
46  
47 (45) MacLeod, A. M.; Mitchell, D. R.; Palmer, N. J.; Van de Poel, H.; Conrath, K.; Andrews,  
48  
49 M.; Leyssen, P.; Neyts, J. Identification of a Series of Compounds with Potent Antiviral Activity  
50  
51 for the Treatment of Enterovirus Infections. *ACS Medicinal Chemistry Letters* **2013**, *4*, 585-589.  
52  
53  
54  
55  
56  
57  
58  
59  
60

1  
2  
3 (46) Compound **5** has an IC<sub>50</sub> of 42 nM against PI4KIIIβ (UCB data). Further profiling revealed  
4 that **5** is inactive (IC<sub>50</sub> > 9 μM) against all other lipid kinases tested<sup>34</sup>.  
5  
6

7 (47) Compound **9** has an IC<sub>50</sub> of 8 nM against PI4KIIIβ, whilst **11** has an IC<sub>50</sub> of 4 nM (UCB  
8 data). Both compounds were reported as having >10000 selectivity for PI4KIIIβ over all other  
9 lipid kinases<sup>41</sup>.  
10  
11  
12

13 (48) Roden, D. M. Drug-Induced Prolongation of the QT Interval. *The New England Journal of*  
14 *Medicine* **2004**, *350*, 1013-1022.  
15  
16  
17

18 (49) Wrighton, S. A.; Vandenbranden, M.; Stevens, J. C.; Shipley, L. A.; Ring, B. J.; Rettie, A.  
19 E.; Cashman, J. R. In Vitro Methods for Assessing Human Hepatic Drug Metabolism: Their use  
20 in Drug Development. *Drug Metabolism Reviews* **1993**, *25*, 453-484.  
21  
22  
23  
24

25 (50) For the 250 kinases tested at Invitrogen see the accompanying supporting information.  
26  
27

28 (51) For the dose response data of **13** and **22** against the 12 lipid kinases tested see the  
29 accompanying supporting information.  
30  
31  
32

33 (52) Braccini, L.; Ciruolo, E.; Campa, C. C.; Perino, A.; Longo, D. L.; Tibolla, G.; Pregnolato,  
34 M.; Cao, Y.; Tassone, B.; Damilano, F.; Laffargue, M.; Calautti, E.; Falasca, M.; Norata, G. D.;  
35 Backer, J. M.; Hirsch, E. PI3K-C2gamma is a Rab5 Effector Selectively Controlling Endosomal  
36 Akt2 Activation Downstream of Insulin Signalling. *Nature Communications* **2015**, *6*, 7400.  
37  
38  
39  
40

41 (53) Mountford, S. J.; Zheng, Z.; Sundaram, K.; Jennings, I. G.; Hamilton, J. R.; Thompson, P.  
42 E. Class II but not Second Class: Prospects for the Development of Class II PI3K Inhibitors. *ACS*  
43 *Medicinal Chemistry Letters* **2015**, *6*, 3-6.  
44  
45  
46  
47

48 (54) Neumann, C. M.; Oughton, J. A.; Kerkvliet, N. I. Anti-CD3 Induced T-cell Activation in  
49 Vivo: Flow Cytometric Analysis of Dose-Responsive, Time-Dependent, and Cyclosporin A  
50  
51  
52  
53  
54  
55  
56  
57  
58  
59  
60

1  
2  
3 Sensitive Parameters of CD4+ and CD8+ Cells from the Draining Lymph Nodes of C57Bl/6  
4 Mice. *International Journal of Immunopharmacology* **1992**, *14*, 1295-1304.

7 (55) Berek, C.; Griffiths, G. M.; Milstein, C. Molecular Events During Maturation of the  
8 Immune Response to Oxazolone. *Nature* **1985**, *316*, 412-418.

11 (56) Vehicle treated animals would normally reject an allograft within 7-10 days of surgery.

14 (57) Ingulli, E. Mechanism of Cellular Rejection in Transplantation. *Pediatric Nephrology*  
15 *(Berlin, Germany)* **2010**, *25*, 61-74.

18 (58) Strumberg, D. Preclinical and Clinical Development of the Oral Multikinase Inhibitor  
19 Sorafenib in Cancer Treatment. *Drugs of Today (Barcelona, Spain: 1998)* **2005**, *41*, 773-784.

22 (59) Skipper, P. L.; Kim, M. Y.; Sun, H. L.; Wogan, G. N.; Tannenbaum, S. R. Monocyclic  
23 Aromatic Amines as Potential Human Carcinogens: Old is New Again. *Carcinogenesis* **2010**, *31*,  
24 50-58.

27 (60) Hodgman, M. J.; Garrard, A. R. A Review of Acetaminophen Poisoning. *Critical Care*  
28 *Clinics* **2012**, *28*, 499-516.

31 (61) Mini AMES test was conducted by Charles River up to a top concentration of 1667 µg per  
32 plate. Some precipitation was observed at the highest 2 concentrations (500 and 1667 µg). Three  
33 strains used were TA 1537, TA 98 and TA 100 in the presence and absence of metabolic  
34 activation (+/-S9).

37 (62) Thompson, D. C.; Josephy, P. D.; Chu, J. W.; Eling, T. E. Enhanced Mutagenicity of  
38 Anisidine Isomers in Bacterial Strains Containing Elevated N-acetyltransferase Activity.  
39 *Mutation Research* **1992**, *279*, 83-89.

42 (63) Both KCN and GSH trapping experiments were conducted in isolated human liver  
43 microsomes. For details see the accompanying supporting information.

1  
2  
3 (64) Lovering, F.; Bikker, J.; Humblet, C. Escape From Flatland: Increasing Saturation as an  
4 Approach to Improving Clinical Success. *Journal of Medicinal Chemistry* **2009**, *52*, 6752-6756.

5  
6  
7 (65) Saal, C.; Petereit, A. C. Optimizing Solubility: Kinetic Versus Thermodynamic Solubility  
8 Temptations and Risks. *European Journal of Pharmaceutical Sciences: Official Journal of the*  
9  
10  
11  
12  
13 *European Federation for Pharmaceutical Sciences* **2012**, *47*, 589-595.

14  
15 (66) Compound **44** was tested in the AMES MPF format against Bacteria (Salmonella  
16 typhimurium) strains TA98, TA100, TA1535, TA1537 and E.coli (uvrA). After 2 days  
17 incubation with and without metabolic activation up to the top concentration of 2000  $\mu\text{M}$ , no  
18  
19  
20  
21  
22  
23 mutagenic effect was observed.

24 (67) Both KCN and GSH trapping experiments were conducted in isolated human liver  
25  
26  
27  
28  
29  
30  
31  
32  
33  
34  
35  
36  
37  
38  
39  
40  
41  
42  
43  
44  
45  
46  
47  
48  
49  
50  
51  
52  
53  
54  
55  
56  
57  
58  
59  
60  
microsomes. For details see accompanying supplemental information.

(68) 2-Methyl-4-methoxy aniline.HCl salt was tested in the AMES MPF format against Bacteria  
(Salmonella typhimurium) strains TA 98, TA 100 and TA 1537. After 2 days incubation with  
and without metabolic activation up to the top concentration of 1000  $\mu\text{M}$ , no mutagenic effect  
was observed.

(69) Selectivity ratios for PI4KIII $\beta$  over the lipid kinase family for compound **44** were generated  
using IC<sub>50</sub> data provided by Life Technologies. The IC<sub>50</sub> against PI4KIII $\beta$  measured at Life  
Technologies for **44** was 5 nM.

(70) Proteros: <http://www.proteros.com/> accessed May 23<sup>rd</sup>, 2018.

(71) For a figure detailing the difference in the level of order/disorder of Chain A and Chain B  
see the supporting information.

(72) Bloom, J. W.; Raju, R. K.; Wheeler, S. E. Physical Nature of Substituent Effects in XH/ $\pi$   
Interactions. *Journal of Chemical Theory and Computation* **2012**, *8*, 3167-3174.

1  
2  
3 (73) (3*R*)-4-(6-Amino-1-methyl-pyrazolo[3,4-*d*]pyrimidin-4-yl)-*N*-(4-methoxy-2-methyl-phenyl)  
4 -3-methyl-piperazine-1-carboxamide, was synthesised in an analogous fashion to **44** using  
5 commercial 2-(*R*)-methyl-4-(tertbutoxycarbonyl)piperazine. It was found to have an IC<sub>50</sub> of 1  
6 μM against PI4KIIIβ and 3 μM in the HuMLR.  
7  
8  
9

10  
11  
12 (74) Groom, C. R.; Bruno, I. J.; Lightfoot, M. P.; Ward, S. C. The Cambridge Structural  
13 Database. *Acta Crystallographica Section B, Structural Science, Crystal Engineering and*  
14 *Materials* **2016**, *72*, 171-179.  
15  
16  
17

18  
19 (75) Sadowski, J.; Gasteiger, J.; Klebe, G. Comparison of Automatic Three-Dimensional Model  
20 Builders Using 639 X-Ray Structures. *Journal of Chemical Information and Computer Sciences*  
21 **1994**, *34*, 1000-1008.  
22  
23  
24

25  
26 (76) Harder, E.; Damm, W.; Maple, J.; Wu, C.; Reboul, M.; Xiang, J. Y.; Wang, L.; Lupyran, D.;  
27 Dahlgren, M. K.; Knight, J. L.; Kaus, J. W.; Cerutti, D. S.; Krilov, G.; Jorgensen, W. L.; Abel,  
28 R.; Friesner, R. A. OPLS3: A Force Field Providing Broad Coverage of Drug-Like Small  
29 Molecules and Proteins. *Journal of Chemical Theory and Computation* **2016**, *12*, 281-296.  
30  
31  
32

33  
34 (77) Friesner, R. A.; Banks, J. L.; Murphy, R. B.; Halgren, T. A.; Klicic, J. J.; Mainz, D. T.;  
35 Repasky, M. P.; Knoll, E. H.; Shelley, M.; Perry, J. K.; Shaw, D. E.; Francis, P.; Shenkin, P. S.  
36 Glide: A New Approach for Rapid, Accurate Docking and Scoring. 1. Method and Assessment  
37 of Docking Accuracy. *Journal of Medicinal Chemistry* **2004**, *47*, 1739-1749.  
38  
39  
40

41  
42 (78) Devos, T.; Sprangers, B.; Lin, Y.; Li, S.; Yan, Y.; Landuyt, W.; Lenaerts, C.; Rutgeerts, O.;  
43 Goebels, J.; Bullens, D.; De Wolf-Peeters, C.; Mathieu, C.; Waer, M.; Billiau, A. D. Occurrence  
44 of Autoimmunity after Xenothymus Transplantation in T-cell Deficient Mice Depends on the  
45 Thymus Transplant Technique. *Transplantation* **2008**, *85*, 640-644.  
46  
47  
48  
49  
50  
51  
52  
53  
54  
55  
56  
57  
58  
59  
60



(79) For a more detailed explanation of the protein production process to facilitate crystallography see the accompanying supporting information.

(80) For details of the model used see the accompanying supporting information.

(81) Murshudov, G. N.; Vagin, A. A.; Dodson, E. J. Refinement of Macromolecular Structures by the Maximum-Likelihood Method. *Acta Crystallographica. Section D, Biological Crystallography* **1997**, *53*, 240-255.

(82) Emsley, P.; Cowtan, K. Coot: Model-Building Tools for Molecular Graphics. *Acta Crystallographica. Section D, Biological Crystallography* **2004**, *60*, 2126-2132.

(83) Molecular Networks GmbH, Germany and Altamira, LLC, USA

(84) Murshudov, G. N.; Skubak, P.; Lebedev, A. A.; Pannu, N. S.; Steiner, R. A.; Nicholls, R. A.; Winn, M. D.; Long, F.; Vagin, A. A. REFMAC5 for the Refinement of Macromolecular Crystal Structures. *Acta Crystallographica. Section D, Biological Crystallography* **2011**, *67*, 355-367.

Graphic for table of contents:

